Ultra-calcic Magmas Generated from Ca-depleted Mantle: an Experimental Study on the Origin of Ankaramites

MAX W. SCHMIDT[1]*, DAVID H. GREEN[2] AND WILLIAM O. HIBBERSON[2]

[1]INSTITUTE OF MINERALOGY AND PETROLOGY, ETH ZURICH, 8092 ZURICH, SWITZERLAND

[2]RESEARCH SCHOOL OF EARTH SCIENCES, ANU, CANBERRA, A.C.T. 0200, AUSTRALIA

RECEIVED JANUARY 1, 2003; ACCEPTED JULY 31, 2003

Ultra-calcic ankaramitic magmas or melt inclusions are ubiquitous in arc, ocean-island and mid-ocean ridge settings. They are primitive in character ($X_{Mg} > 0{\cdot}65$) and have high CaO contents (>14 wt %) and CaO/Al_2O_3 (>1·1). Experiments on an ankaramite from Epi, Vanuatu arc, demonstrate that its liquidus surface has only clinopyroxene at pressures of 15 and 20 kbar, with X_{CO_2} in the volatile component from 0 to 0·86. The parental Epi ankaramite is thus not an unfractionated magma. However, forcing the ankaramite experimentally into saturation with olivine, orthopyroxene and spinel results in more magnesian, ultra-calcic melts with CaO/Al_2O_3 of 1·21–1·58. The experimental melts are not extremely Ca-rich but high in CaO/Al_2O_3 and in MgO (up to 18.5 wt %), and would evolve to high-CaO melts through olivine fractionation. Fractionation models show that the Epi parent magma can be derived from such ultra-calcic experimental melts through mainly olivine fractionation. We show that the experimental ultra-calcic melts could form through low-degree melting of somewhat refractory mantle. The latter would have been depleted by previous melt extraction, which increases the CaO/Al_2O_3 in the residue as long as some clinopyroxene remains residual. This finding corrects the common assumption that ultra-calcic magmas must come from a Ca-rich pyroxenite-type source. The temperatures necessary for the generation of ultra-calcic magmas are ≥1330°C, and their presence would suggest melting regimes that are at the upper temperature end of previous interpretations made on the basis of picritic magmas.

KEY WORDS: *ankaramite; refractory lherzolite; ultra-calcic magma*

INTRODUCTION

Ultra-calcic magmas or ankaramites (CaO/Al_2O_3 weight ratio ≥1·1) occur as lavas in the Vanuatu arc (Barsdell, 1988; Barsdell & Berry, 1990); similar compositions occur as melt inclusions in rocks of several other arcs (Schiano *et al.*, 2000). Olivine phenocrysts with $X_{Mg} > 90$, and coexisting chrome-rich or aluminous spinel, identify the Vanuatu ankaramites as primitive magmas. There are similarities in composition between island-arc ankaramite lavas and ultra-calcic melt inclusions in magnesian olivines from arcs, ocean-island and mid-ocean ridges (Fig. 1). Ultra-calcic melts have been divided into two groups (Schiano *et al.*, 2000; Kogiso & Hirschmann, 2001): a relatively alkali-poor, silica-rich hypersthene-normative suite ($Na_2O + K_2O$ generally ≤3 wt %, $SiO_2 > 48$ wt %) and an alkali-rich, silica-poor nepheline-normative suite ($Na_2O + K_2O$ = 2·5–6 wt %; SiO_2 as low as 45 wt %). The latter is found uniquely in the arc environment, whereas the hypersthene-normative type occurs in arcs, ocean islands and mid-ocean ridge settings (Schiano *et al.*, 2000).

The Vanuatu ankaramite lavas range from slightly nepheline-normative (island of Gaua) to hypersthene + olivine normative, and for this study we have chosen the hypersthene-normative Epi suite for investigation (Barsdell & Berry, 1990). The purpose of this study is to test whether these ultra-calcic magmas may be derived from lherzolitic or harzburgitic mantle sources. We emphasize that, on the island of Epi, ankaramite magma volumes are at a 10–100 km^3 scale and that

*Corresponding author. Telephone: xx41-1-632-7988. Fax: xx41-1-632-1088. E-mail: max.schmidt@erdw.ethz.ch

Journal of Petrology 45(3)

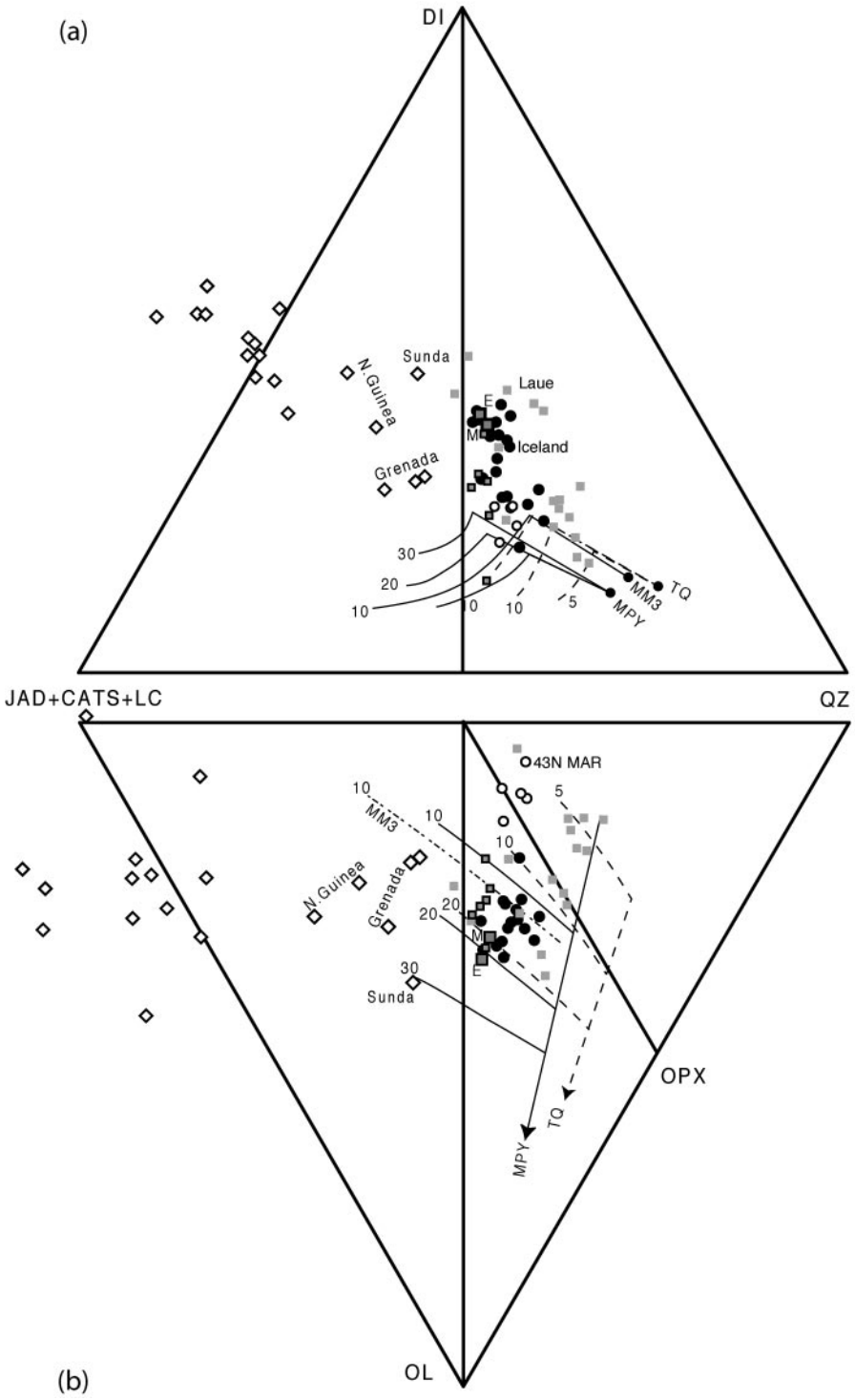

Fig. 1. Ultra-calcic melt compositions projected on two faces of the modified basalt tetrahedron (Yoder & Tilley, 1962; Falloon *et al*., 1999). (a) Projection from olivine; (b) projection from diopside. Ultra-calcic melts as reported in the literature. ◇, nepheline-normative alkaline-rich ultra-calcic melts [compiled by Schiano *et al*. (2000)]. All other symbols are hypersthene-normative alkali-poor melts. Grey filled squares, Epi and Merelava, Vanuatu arc; large grey filled squares, parental magmas from Epi (E) and Merelava (M) (Barsdell, 1988; Barsdell & Berry, 1990). Grey squares without black borders, Lau basin (Kamenetsky *et al*., 1997); ●, Iceland (Sigurdsson *et al*., 2000; Slater *et al*., 2001); ○, Mid-Atlantic Ridge at 43°N (Kamenetsky *et al*., 1998). Also shown are melting curves for mid-ocean ridge pyrolite (MPY) and refractory Tinaquillo lherzolite (TQ) from Falloon *et al*. (1988, 1999), and lherzolite MM3 from Hirschmann *et al*. (1998); numbers indicate pressures in kbar.

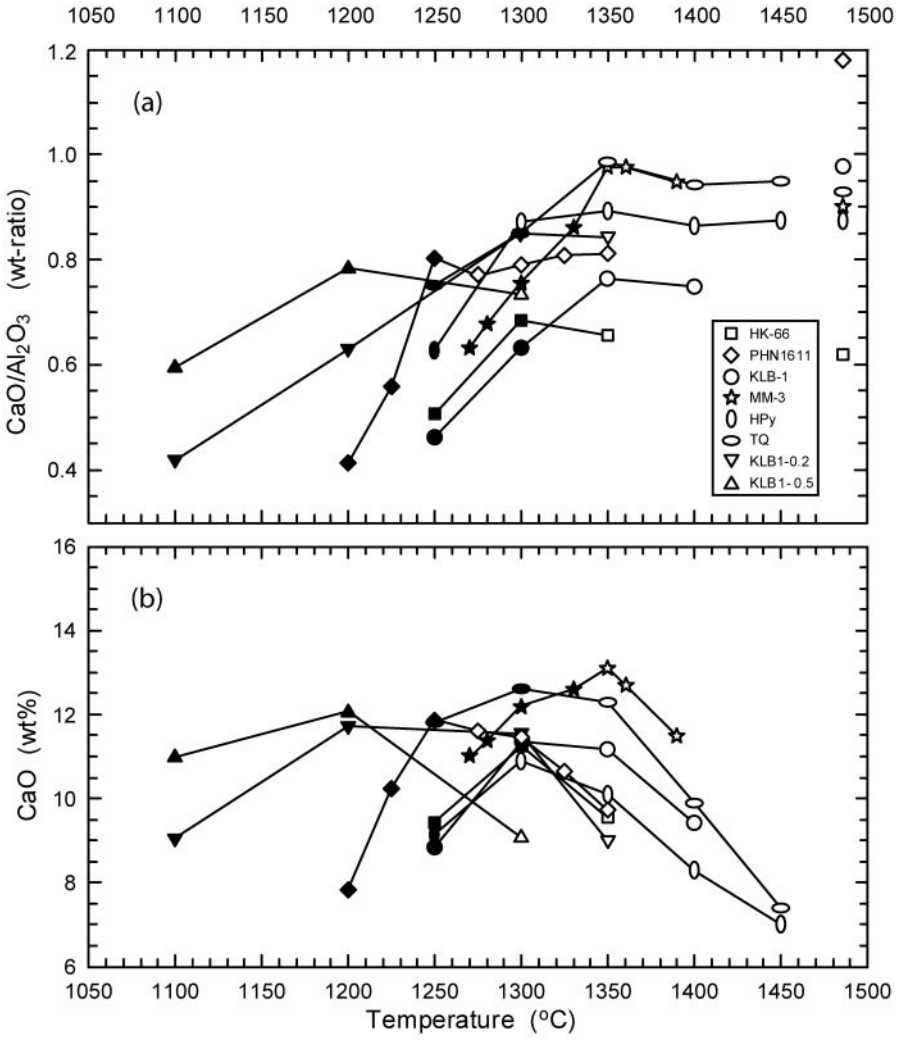

Fig. 2. (a) CaO/Al_2O_3 weight ratio and (b) CaO (wt %) in melts vs temperature from experimental studies of lherzolites. Filled symbols, cpx + opx + ol + sp + melt; open symbols, opx + ol + sp + melt residue. Maxima in CaO and shoulders in CaO/Al_2O_3 correspond to the clinopyroxene-out reaction, the temperature of which correlates with the 'fertility' of the bulk composition. Bulk CaO/Al_2O_3 is indicated at the right-hand side in (a). HK66 and KLB-1 are from Hirose & Kushiro (1993); KLB1-0.2 and KLB1-0.5 are from Hirose & Kawamoto (1995); PHN 1611 is from Kushiro (1996); KLB-1 is from Takahashi *et al.* (1993); MM3 is from Hirschmann *et al.* (1998) and Falloon *et al.* (1999); HPy and TQ are from Falloon *et al.* (1988).

melt inclusions that occur at grain-size scales (and may or may not reflect large-scale processes) may result from very different processes (Kamenetsky *et al.*, 1998). The bulk-rock compositions of island-arc ankaramites may be influenced by accumulation and/or fractionation of olivine, clinopyroxene and chrome spinel phenocrysts. However, previous workers have used petrographic criteria and known crystal partitioning relationships to infer the liquid compositions required to precipitate the observed olivine (Mg_{94}), diopside (Mg_{94}) and chrome spinel phenocrysts (Barsdell, 1988; Barsdell & Berry, 1990; Eggins, 1993). These liquid compositions are our starting point for the experimental study and we use an olivine-rich ankaramite from Western Epi (sample 71046, Barsdell & Berry, 1990) that is close to the estimated parent magmas for Western Epi and Meralava (Barsdell & Berry, 1990) as a primitive, hypersthene-normative ultra-calcic magma.

The melting of lherzolitic mantle is experimentally well studied (Figs 1 and 2). Anhydrous batch melting of fertile or slightly refractory lherzolite cannot yield magmas with CaO/Al_2O_3 significantly higher than unity. In all of the lherzolite melting studies, liquid compositions increase in CaO and CaO/Al_2O_3 up to the point of clinopyroxene disappearance (Fig. 2) leaving orthopyroxene and olivine in the residue. With further melting, they then decrease in CaO more

strongly than in Al_2O_3 through melting of relatively aluminous orthopyroxene, so that the CaO/Al_2O_3 decreases slightly. The maximum CaO/Al_2O_3 of 1·0 at the clinopyroxene-out stage remains far below the values achieved in ultra-calcic magmas (maximum 1·5–1·7). It is thus difficult to obtain ultra-calcic magmas from mantle compositions with excess orthopyroxene (relative to clinopyroxene). Alternatively, melting of Ca-rich bulk compositions such as olivine pyroxenites and wehrlites has been suggested as a mechanism for generating ultra-calcic magmas. Kogiso & Hirschmann (2001) studied the dry melting of various wehrlitic compositions and obtained ultra-calcic melts. However, these melts were nepheline-normative, were obtained only at melt fractions above 30% (see Discussion) and were unsuitable as parents to the ultra-calcic melt inclusions, leading Kogiso & Hirschmann to discuss the possibility of obtaining ultra-calcic melts from depleted peridotite.

Dissolved CO_2 could shift the olivine + orthopyroxene + clinopyroxene + spinel saturation surface to higher normative diopside and CaO/Al_2O_3 than for H_2O-bearing or dry melting processes. In the study of Brey & Green (1977), dissolved $(CO_3)^{2-}$ and $(OH)^-$ caused melilitites to saturate in orthopyroxene in addition to clinopyroxene + olivine, allowing olivine melilitite to form from residual garnet lherzolite at pressures of 25–35 kbar. Our experimental approach was to determine the influence of variable CO_2 and H_2O on temperature and phase relationships at the liquidus of a parental island-arc ankaramite with the scope to produce melts with high normative diopside and CaO/Al_2O_3. In a second step, we designed our methods to force the parental Epi melt into saturation with olivine, orthopyroxene and spinel with varying CO_2:H_2O in the dissolved volatile component. The objective was to find a melt composition for each CO_2:H_2O just at the elimination of clinopyroxene from the residue, i.e. at the temperature at which the highest CaO contents and CaO/Al_2O_3 necessarily occur.

In the following we use 'ultra-calcic' for melts with a weight ratio CaO/Al_2O_3 >1·1 irrespective of the CaO content (we will show that high CaO/Al_2O_3 is the essential characteristic of parental ultra-calcic magmas; high CaO can be achieved in a later step).

EXPERIMENTAL TECHNIQUES AND STRATEGY

Liquidus experiments

As a first step, the liquidus surface of the parental Epi magma (Barsdell & Berry, 1990) was determined as a function of volatile composition. Two H_2O–CO_2 sections were investigated at 15 and 20 kbar (Table 2). This pressure range is based on the absence of garnet in the source of the Epi ankaramites (Barsdell & Berry, 1990), which results in an upper pressure limit of *c.* 25 kbar. The thickness of the intra-oceanic arc crust beneath the Vanuatu arc is not well known, but in the very similar Izu–Bonin–Mariana arc system, it is >20 km (Suyehiro *et al.*, 1996). This sets a lower pressure limit for mantle melting of roughly 10 kbar, assuming that the Epi magmas are mantle-derived.

A glass with a composition equivalent to the Epi parental magma (Table 1) but deficient in MgO was prepared at controlled oxygen fugacity to obtain an Fe^{3+}/Fe^{tot} of 0·2. The deficiency in MgO was then compensated for by adding previously dried $Mg(OH)_2$ and/or $MgCO_3$. This procedure results in a constant molar volatile/non-volatile oxide ratio and in a varying X_{CO_2} in the volatile component. Addition of $Mg(OH)_2$ only resulted in 4·1 wt % H_2O and $X_{CO_2} = 0·0$ in the starting material. Addition of reagent grade $MgCO_3$ always results in addition of some H_2O as well, as synthetic $MgCO_3$ is difficult to dry without causing decarbonization. We determined the H_2O content of $MgCO_3$ to be 3·1 wt % after drying at 110°C. This results in 9·3 wt % CO_2 + 0·57 wt % H_2O and $X_{CO_2} = 0·87$ for addition of '$MgCO_3$ only' to the MgO-deficient glass. Batches with the original MgO content of the Epi parental magma were prepared with $CO_2/(H_2O + CO_2)$ fractions of 0·0, 0·24, 0·46, 0·66, 0·78 and 0·87. Primitive arc magmas generally do not contain more than 2–3 wt % H_2O (Sobolev & Chaussidon, 1996) and our high volatile contents were chosen to maximize the effect of volatiles on the liquidus within reasonable bounds. Experiments were performed in an end-loaded $\frac{1}{2}$-inch piston cylinder apparatus using a standard salt–Pyrex–graphite–crushable alumina assemblage. The inner furnace diameter was 3·2 mm and the capsules were separated from the furnace by an alumina sleeve. A PtRh type-B thermocouple was used for temperature measurement. Most experiments were conducted in welded graphite–Pt double capsules (1·0 mm i.d. graphite, 1·8 mm i.d. Pt, 2·3 mm o.d. Pt). Run times were 30 or 60 min. The high temperatures of this experimental study resulted in reducing conditions within graphite capsules, and a few experiments were repeated in welded 2·0 mm o.d. $Au_{80}Pd_{20}$ capsules. Fe loss to the $Au_{80}Pd_{20}$ capsule was insignificant (see below) and melt compositions in superliquidus experiments were identical to initial bulk compositions within analytical uncertainty.

Saturation experiments

A second set of experiments was designed to force the parental Epi melt into saturation with olivine,

Table 1: Bulk compositions and starting materials

	Peridotites			Minerals in mix 2 synthesized at 1200°C, 2 GPa				Bulk* sandwich 40% mix 2 + 60%(71046 + 5% ol†)	Epi parent	
	mix 2	mix 4	mix 3	ol	opx	cpx	sp		71046	71046 + 5% ol†
SiO_2	46·60	49·82	50·33	41·00	57·24	54·68	0·23	47·90	49·15	48·73
TiO_2	0·08	0·06	0·06	0·02	0·04	0·11	0·98	0·26	0·40	0·38
Al_2O_3	1·40	1·47	1·48	0·02	0·26	1·03	12·61	7·28	11·76	11·16
Cr_2O_3	6·19	1·91	0·92	0·41	0·69	1·59	49·23	2·53	0·10	0·10
Fe_2O_3	—	—	—	0·00	0·43	0·00	9·18	—	—	—
FeO	7·71‡	7·27‡	7·34‡	8·43	3·49	3·04	13·02	8·36‡	8·74*‡	8·77*‡
MgO	34·04	35·22	35·58	49·66	34·09	21·26	14·05	22·89	13·77	15·59
CaO	3·95	4·22	4·26	0·28	3·07	18·28	0·25	9·97	14·67	13·93
Na_2O	0·03	0·03	0·03	0·00	0·00	0·14	0·00	0·64	1·11	1·05
K_2O	0·00	0·00	0·00	0·00	0·00	0·00	0·00	0·17	0·30	0·29
Total	100·0	100·0	100·0	99·7	99·3	100·1	99·6	100·0	100·0	100·0
CaO/Al_2O_3§	2·82	2·87	2·88					1·37	1·25	1·25
X_{Mg}¶	0·887	0·896	0·896	0·913	0·946	0·926	0·631	0·831	0·733	0·760
X_{Cr}¶	0·748	0·466	0·294	—	0·639	0·509	0·724	0·187	0·006	0·006
Mode**				24·6	51·5	12·6	11·3			

*Exact bulk composition varies as a result of slightly different peridotite:ankaramite layer thicknesses.
†+5% ol means 5 wt % of San Carlos olivine added.
‡Total Fe as FeO.
§Weight ratio.
¶Molar coefficients $MgO/(MgO + FeO)$ and $Cr_2O_3/(Cr_2O_3 + Al_2O_3)$.
**Weight percent.

orthopyroxene, clinopyroxene and spinel under a range of X_{CO_2} values of the dissolved volatile component (Table 3). The objective of this series was to determine melt compositions at the temperature at which clinopyroxene disappears from the solid residue for each X_{CO_2}.

A layer of Epi melt starting material was placed below a peridotite layer within the capsule(s), maintaining a roughly constant peridotite:ankaramite proportion of 4:6 (Table 3). The peridotite was synthesized from an oxide + iron mix at 10 kbar, 1200°C. The resulting fine-grained (<10 μm) mix of olivine, enstatite, diopside and spinel (for actual mineral compositions and proportions, see Table 1) was finely ground before further use as a peridotite layer. The bulk composition of the refractory peridotite layer was based on mineral compositions from the phenocryst phases of a high Ca-boninite (Tongan Arc, Sobolev & Danyushevsky, 1994, sample 26-2), which are thought to be appropriate for refractory melt-depleted mantle. The synthetic peridotite had low clinopyroxene and high orthopyroxene contents because the ankaramite melt-layer was already clinopyroxene saturated, but considerable dissolution of orthopyroxene in the melt was expected. The first two experiments revealed dissolution fronts of olivine within the peridotite layer so that the melt layer was not in contact with olivine. To ensure unzoned capsules and that all melts were in contact (and thus saturated) with olivine, all subsequent experiments had an additional 5 wt % San Carlos olivine ($X_{Mg} = 0{\cdot}90$) mixed into the melt layer. These experiments (Table 3) did not show any zonation in the peridotite layer.

With this experimental setup we were able to obtain melt and mineral compositions at 15 kbar for X_{CO_2} values of 0·0, 0·24, 0·46, 0·66 and 0·78 for melts saturated in ol–opx–cpx–sp and, within a temperature interval of 20°C, melts saturated in ol–opx–sp. A series of experiments was also performed with a dry glass, i.e. a volatile-absent bulk composition, that was directly fused from oxides. Experiments carried out with welded graphite–Pt double capsules yielded low oxygen fugacities (from $f_{O_2} \leq QFM - 2{\cdot}7 = IW + 0{\cdot}9$ at 1290°C to $X_{CO_2} \leq QFM - 2{\cdot}9 = IW + 0{\cdot}6$ at 1415°C, where QFM is quartz–fayalite–magnetite and IW is iron–wüstite). Because of the presence of graphite,

Table 2: Liquidus experiments on Epi parent melt

Run no.	Capsule	X_{CO_2}	P (kbar)	T (°C)	t (h)	Result*
D-19	Pt + graph	0·00	20	1350	1	cpx + liq
D-29	Pt + graph	0·00	20	1370	1	(liq) all qq
D-27	Pt + graph	0·24	20	1360	1	cpx + liq/(liq) all qq
D-2	Pt + graph	0·46	20	1300	0·5	cpx + liq
D-3	Pt + graph	0·46	20	1360	0·5	cpx + liq
D-6	Pt + graph	0·46	20	1380	0·5	cpx + liq
D-11	Pt + graph	0·46	20	1390	1	liq
D-4	Pt + graph	0·46	20	1400	0·5	liq
D-5	Pt + graph	0·66	20	1380	1	cpx + liq
D-9	Pt + graph	0·66	20	1390	1	cpx + liq
D-8	Pt + graph	0·66	20	1400	1	liq
D-10	Pt + graph	0·78	20	1400	1	cpx + liq/liq
D-16	Pt + graph	0·78	20	1415	1	liq
D-28	Pt + graph	0·86	20	1400	1	very few cpx + liq/liq
D-21	Pt + graph	0·86	20	1415	1	liq
E-26	Pt + graph	0·00	15	1300	1	cpx + liq
D-95	Pt + graph	0·00	15	1290	1	cpx + liq
D-26	Pt + graph	0·24	15	1340	1	liq
D-35	Pt + graph	0·24	15	1315	1	equ-cpx(?)/(liq) all qq
E-27	Pt + graph	0·24	15	1300	1	cpx + liq
D-54	Pt + graph	0·46	15	1340	0·5	liq
D-55	Pt + graph	0·46	15	1315	0·5	liq
D-99	Pt + graph	0·46	15	1295	1	cpx + liq
D-12	Pt + graph	0·46	15	1360	1	cpx + liq
D-15	Pt + graph	0·46	15	1380	1	cpx + liq/liq
D-18	Pt + graph	0·46	15	1390	1	liq
D-33	Pt + graph	0·66	15	1320	1	cpx + liq/liq
D-32	Pt + graph	0·66	15	1340	1	liq
D-24	Pt + graph	0·66	15	1360	1	liq
D-22	Pt + graph	0·66	15	1375	1	liq
D-46	Pt + graph	0·78	15	1320	1	cpx + liq/liq
D-38	Pt + graph	0·78	15	1330	1	liq
D-34	Pt + graph	0·78	15	1350	1	liq
D-25	Pt + graph	0·78	15	1370	1	liq
D-23	Pt + graph	0·78	15	1385	1	liq
D-52	$Au_{80}Pd_{20}$	0·24	15	1275	0·5	cpx + liq
D-48	$Au_{80}Pd_{20}$	0·24	15	1305	0·5	liq
D-53	$Au_{80}Pd_{20}$	0·66	15	1290	0·5	cpx + liq
D-49	$Au_{80}Pd_{20}$	0·66	15	1315	0·5	liq

*A slash separates assemblages in capsules with two zones. qq, mostly dendritic quench clinopyroxene with some interstitial liquid.

redox exchange between C–H–O species dissolved in the melt and the capsule occurs. We have not as yet been able to obtain direct CO_3^{2-} and OH^- contents of the glass pools (by IR spectroscopy) and in the following, X_{CO_2} and X_{H_2O} values refer to the initial mixes. To avoid the graphite capsule and reducing conditions, a few runs were repeated employing welded $Au_{80}Pd_{20}$ single capsules, with the intention that during relatively short run times the initial Fe^{3+}/Fe^{tot} should more or less be maintained. After the experiment, Fe was measured in the AuPd capsules. A zone of 20–40 μm width with Fe above detection limit was identified; the maximum measured Fe content in the metal was 0·4 wt %, resulting in insignificant Fe loss to the sample.

Recently, it was suggested (Liu & O'Neill, 2002) that Cr/Al of the source may significantly influence the Ca/Al of melt compositions without significant increase of the Cr_2O_3 concentration in the melt. To evaluate this parameter, two additional peridotite mixes with (molar) $X_{Cr} = Cr_2O_3/(Cr_2O_3 + Al_2O_3) = 0{\cdot}466$ and 0·294 were prepared, i.e. with Cr_2O_3 contents lower than our initial mix (with $X_{Cr} = 0{\cdot}748$). The experimental 'clinopyroxene-out bracket' at $X_{CO_2} = 0{\cdot}78$ and a bulk X_{Cr} of approximately 0·187 (exact bulk compositions depend on the exact peridotite: ankaramite layer thicknesses) was repeated at identical conditions but with bulk X_{Cr} of 0·066 and 0·033 (Tables 1 and 3).

EXPERIMENTAL RESULTS

The liquidus of the Epi ankaramite 'parental' magma

Clinopyroxene is the single liquidus phase for all investigated X_{CO_2} at 15 and 20 kbar (Fig. 3). Liquidus temperatures rise from 1300 to 1330°C with X_{CO_2} increasing from 0·0 to 0·87 at 15 kbar and from 1360 to 1410°C with X_{CO_2} increasing from 0·0 to 0·87 at 20 kbar. Characteristically, the first experiment below the liquidus temperature has 50–70% clinopyroxene present, although this observation may be moderated by some quench rim growth on primary clinopyroxene. Dendritic quench clinopyroxene is always abundant in the interstitial melt, and, in pools of melt, 50–200 μm wide zones of quench clinopyroxene are common. The most extreme examples of high degrees of crystallization over a small temperature interval occur in experiments (e.g. D-33, 1320°C, 15 kbar, Fig. 4) in which it appeared that one part of the capsule was at superliquidus conditions (the measured melt composition in this part being that of the bulk composition) and the remainder of the capsule contained >50% clinopyroxene crystals. The crystallization of clinopyroxene in only one part of the capsule is ascribed to a temperature gradient over the capsule length (typically 1·2–1·5 mm inner length) and cannot be attributed to chemical differentiation within the capsule. The

Table 3: Saturation experiments at 15 kbar

Run no.	Capsule	X_{CO_2}	T (°C)	t (h)	Perid. (%)*	Result		
						Peridotite layer	Melt layer	Bottom
E-8	$Au_{80}Pd_{20}$	0·00	1300	4	39	sp–ol–opx–2cpx	melt	2cpx
D-90	$Au_{80}Pd_{20}$	0·00	1315	2	36	sp–ol–opx	melt	—
D-76	Pt–graph	0·24	1330	24	43	sp–ol–opx–2cpx	cpx–melt	—
E-17	Pt–graph	0·24	1340	20·5	47	sp–ol–opx	melt, ol sinking	sp–ol–opx–pig
D-83	Pt–graph	0·24	1350	22	43	sp–ol–opx	melt, opx sinking	sp–ol–opx
D-80	Pt–graph	0·46	1335	24	38	sp–ol–opx–pig	melt	—
D-81	Pt–graph	0·46	1355	22·5	43	sp–ol–opx	melt	sp–ol–opx
E-4	$Au_{80}Pd_{20}$	0·46	1320	4	43	sp–ol–opx–Cacpx	melt	2cpx
D-89	$Au_{80}Pd_{20}$	0·46	1335	2	33	sp–ol–opx/opx	melt	—
D-77	Pt–graph	0·66	1340	24	35	sp–ol–opx–pig	pig–melt	pig
E-16	Pt–graph	0·66	1350	20·5	43	sp–ol–opx	melt, ol + opx sinking	sp–ol–opx
D-84	Pt–graph	0·66	1360	22	45	sp–ol–opx	melt	sp
D-79	Pt–graph	0·78	1345	24	38	sp–ol–opx–pig	pig-melt	sp–pig
D-82	Pt–graph	0·78	1365	22·5	48	sp–ol–opx–pig	melt	sp–pig
E-6	Pt–graph	0·78	1380	19	44	sp–ol–opx	melt	sp–ol–opx
E-30	$Au_{80}Pd_{20}$	0·78	1320	4	40	sp–ol–opx–Cacpx	melt	Cacpx
E-5	$Au_{80}Pd_{20}$	0·78	1335	4	33	sp–opx–ol	melt	sp–opx
D-92	$Au_{80}Pd_{20}$	0·78	1350	2	36	sp(–)–ol-opx	melt	—
D-91	Pt–graph	dry	1375	4	30	sp(–)–ol(–)–pig	melt	pig
E-7	Pt–graph	dry	1375	24	61	sp–ol–opx–pig	melt	sp–ol–pig
G-32	Pt–graph	dry	1400	24	73	sp–ol–opx–pig	melt	sp–ol–pig
D-85	Pt–graph	dry	1400	19	44	sp–ol–pig	melt	—
Peridotite mix4 (intermediate X_{Cr})								
F-16	Pt–graph	0·78	1360	23	40	ol–opx–pig–sp	melt	sp–pig
F-31	Pt–graph	0·78	1380	24	50	ol–opx–sp	melt	ol–opx
Peridotite mix3 (low X_{Cr})								
E-28	Pt–graph	0·78	1340	20·5	43	ol–opx	melt	ol–opx–pig
E-10	Pt–graph	0·78	1365	22	48	ol–opx	melt	ol–opx

*Measured to approximately ±3% during filling of the capsule.

observed extensive crystallization over a narrow temperature interval is similar to the diopside–orthopyroxene–olivine ternary in the CaO–MgO–SiO_2 system in which the interval between super-liquidus and sub-solidus does not exceed 20°C where clinopyroxene is in excess of orthopyroxene and olivine (Kushiro, 1969). The reason for crystallization behaviour similar to that in the simple synthetic system is probably a reflection of the low concentrations of TiO_2 and Na_2O, and, compared with most other mafic magmas, relatively low Al_2O_3 contents of the bulk composition and clinopyroxenes.

The composition of clinopyroxenes at the liquidus surface is in the range 0·62–0·78 Ca p.f.u., 0·10–0·32 Al p.f.u. and $X_{Mg} = 0{\cdot}80$–$0{\cdot}91$ (Table 4). Strong zonation is observed in clinopyroxene, with the highest X_{Mg} and Ca contents and lowest Al contents in the cores. This zonation is a consequence of the large amount of crystallization occurring within an experiment. The first clinopyroxene nucleates in equilibrium with a melt close to the bulk composition. However, as clinopyroxene grows, the residual melt evolves and becomes enriched in Fe, Al and Na. Thus, with increasing degree of crystallization, clinopyroxene crystallizes in equilibrium with an increasingly Fe-, Na- and Al-enriched and Ca- and Mg-depleted melt without diffusional equilibration (Cherniak, 2001) of previously formed clinopyroxene cores. Ca contents of

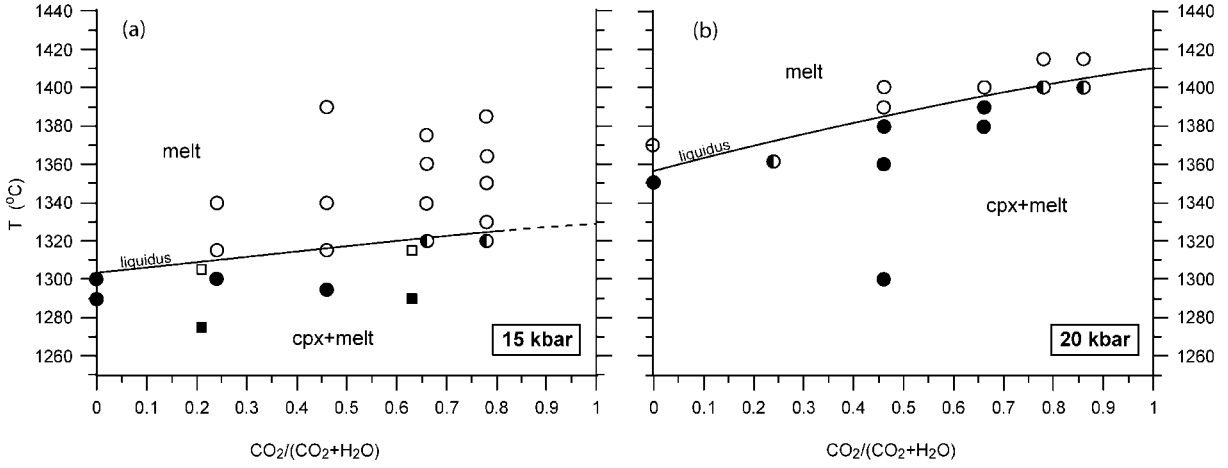

Fig. 3. Liquidus at (a) 15 kbar and (b) 20 kbar of the magma parental to the Epi ankaramites (Table 1, 71046) as a function of X_{H_2O}–X_{CO_2} in the volatile component (for details see text). Filled symbols, equilibrium clinopyroxene + melt; open symbols, melt only; half-filled symbols, one part of the capsule fully molten and above the liquidus, the other part contains clinopyroxene + melt. Circles, experiments in Pt–graphite double capsules; squares, experiments in $Au_{80}Pd_{20}$ single capsules.

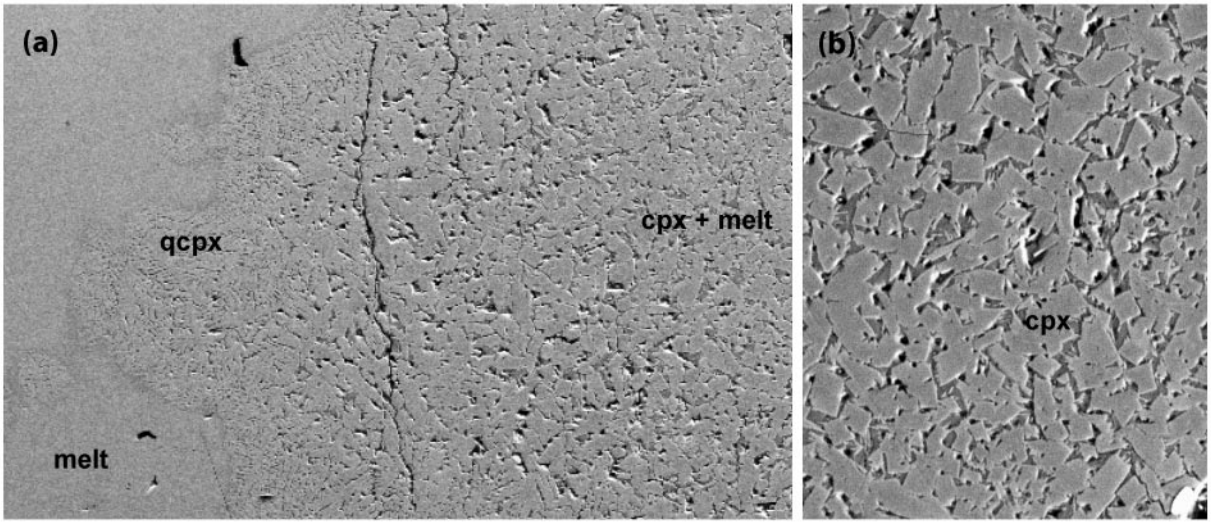

Fig. 4. Back-scattered electron (BSE) images of experiment D10 where (a) the liquidus crosses the capsule as a result of the temperature gradient present. qcpx, quench-clinopyroxene; cpx, equilibrium clinopyroxene (with quench rims). Melt has bulk composition. (b) Detail of clinopyroxene + melt zone.

clinopyroxene on the liquidus decrease with increasing X_{CO_2} from approximately 0·74 to 0·64 Ca p.f.u. Nevertheless, clinopyroxene cores of this series of experiments are at least 0·1–0·2 Ca p.f.u. higher than a clinopyroxene that would lie on the orthopyroxene–clinopyroxene solvus. This might be taken as an indication that even at the highest X_{CO_2} contents of the experiments, we are still 'far' from orthopyroxene saturation.

The conclusion of this series of experiments is that the estimated parental liquid of the Epi ankaramites is not in equilibrium with any possible orthopyroxene-bearing mantle residue over the investigated pressure range. A similar conclusion was reached by Della Pasqua & Varne (1997) who investigated ankaramitic melt inclusions from Rindjani volcano, Indonesia, which have a range of CO_2 and H_2O dissolved in the melts.

Ultra-calcic melts in equilibrium with a mantle restite

To understand the chemical differences between a melt derived from a lherzolite source and the Epi parental magma, a layer of the latter melt was forced into

Table 4: Clinopyroxenes from liquidus experiments

Run:	E26	D99	D46	D19	D9	D19
T (°C):	1300	1295	1320	1350	1390	1330
P (kbar):	15	15	15	20	20	20
n:	6	11	10	6	19	5 quench
SiO_2	53·02	52·73	52·67	54·20	52·18	49·91
TiO_2	0·11	0·14	0·21	0·00	0·11	0·27
Al_2O_3	3·46	4·02	4·41	2·88	5·61	9·94
Cr_2O_3	0·37	0·35	0·40	0·34	0·16	0·21
Fe_2O_3	0·03	0·08	0·00	0·89	0·00	0·00
FeO	4·42	5·22	5·01	3·59	5·43	6·55
MgO	18·49	18·32	18·74	19·18	17·81	16·32
CaO	19·27	18·50	17·91	19·56	17·32	17·12
Na_2O	0·29	0·32	0·31	0·39	0·65	0·44
K_2O	0·01	0·01	0·00	0·00	0·01	0·00
Total	99·5	99·8	99·8	101·2	99·4	100·9
Si	1·928	1·915	1·909	1·936	1·898	1·796
Ti	0·003	0·004	0·006	0·000	0·003	0·007
Al	0·148	0·172	0·189	0·121	0·241	0·422
Cr	0·011	0·010	0·011	0·010	0·005	0·006
Fe^{3+}	0·001	0·002	0·000	0·024	0·000	0·000
Fe^{2+}	0·134	0·159	0·152	0·107	0·165	0·197
Mg	1·002	0·992	1·013	1·021	0·966	0·875
Ca	0·751	0·720	0·696	0·749	0·675	0·660
Na	0·021	0·023	0·022	0·027	0·046	0·031
K	0·001	0·000	0·000	0·000	0·000	0·000
X_{Mg}	0·882	0·862	0·870	0·905	0·854	0·816

$X_{Mg} = Mg/(Mg + Fe^{2+})$. *n*, number of analyses.

saturation with olivine, orthopyroxene and spinel. At each X_{CO_2} and with rising temperature, this second series of experiments resulted in a characteristic succession of three run products (Fig. 5):

(1) at temperatures more than 15°C below the clinopyroxene-out reaction, a large amount of clinopyroxene (30–60%) crystallized in the ankaramite layer, leaving a small melt pool around the rim of the capsule (Fig. 6a and b; D-76, D-77, D-79 in Table 3). In these experiments melt reacted with the peridotite layer to increase modal pyroxene and infiltrated only into the lower portion of the peridotite layer. We cannot be certain that the analysed melts in the melt pool have fully equilibrated with the peridotite layer. The extensive crystallization of clinopyroxene is analogous to that observed in the liquidus experiments and melt compositions from these experiments have relatively low CaO/Al_2O_3 (0·93–1·23).

(2) At temperatures less than 15°C below the clinopyroxene-out reaction, the ankaramite layer was fully molten, interstitial melt was present in the entire peridotite layer and modal amounts of clinopyroxene in the bulk decreased (Fig. 6c and d). In some experiments a layer of clinopyroxene ± spinel was present at the bottom of the capsule.

(3) At temperatures above the clinopyroxene-out reaction, residual orthopyroxene and olivine often grew to grain sizes of 100 μm (Fig. 6e–g). The former peridotite layer was typically reduced to half of its initial thickness and in most experiments a few 100–200 μm crystals of orthopyroxene or olivine were observed. These appeared to have sunk through the melt layer towards the bottom of the capsule (Fig. 6f). At the bottom of the capsules, an orthopyroxene–olivine–spinel layer is present. This layer could result from crystal settling, but could also have formed through a dissolution–reprecipitation process.

Melt compositions

Melt compositions at X_{CO_2} values of 0·00, 0·24, 0·46, 0·66 and 0·78 were measured in experiments in which melts were saturated with olivine–orthopyroxene–clinopyroxene–spinel and with olivine–orthopyroxene–spinel. These are melts that are just below and above the clinopyroxene-out reaction, respectively (Table 5). For each X_{CO_2}, the highest CaO/Al_2O_3 is obtained at the clinopyroxene-out reaction, and melt compositions vary systematically as a function of X_{CO_2} and capsule material. Similar to the liquidus experiments, clinopyroxene in the peridotite layer melts over a narrow (<20°C) temperature interval, causing significant variations in melt compositions just below the clinopyroxene-out reaction as a result of different amounts of coexisting clinopyroxene. In the following, only melt compositions just above the clinopyroxene-out reaction are discussed. These melts all have high CaO/Al_2O_3 ranging from 1·31 at $X_{CO_2} = 0·0$ to a maximum value of 1·57 at $X_{CO_2} = 0·78$. Although CaO/Al_2O_3 is as high as in most natural ultra-calcic melts, the experimental melts do not have extreme CaO contents. CaO contents are in the range 14·1–12·3 wt % and decrease with increasing X_{CO_2}. Al_2O_3 in the melt also decreases with increasing X_{CO_2} (from 10·3 to 7·9 wt %). SiO_2 contents are fairly constant at 50·0 ± 0·8 wt % and melts are hypersthene-normative. The experimental melts have X_{Mg} values ranging from 0·77 to 0·80 and high MgO contents of 16·3–18·6 wt %, the latter increasing with X_{CO_2}. Variation of the peridotite layer X_{Cr} from 0·75 to 0·47 resulted in only minor changes of phase and melt compositions, but with an X_{Cr} value of 0·29 in the peridotite layer spinel was eliminated from the residue and melts remained at high CaO/Al_2O_3 (Table 5).

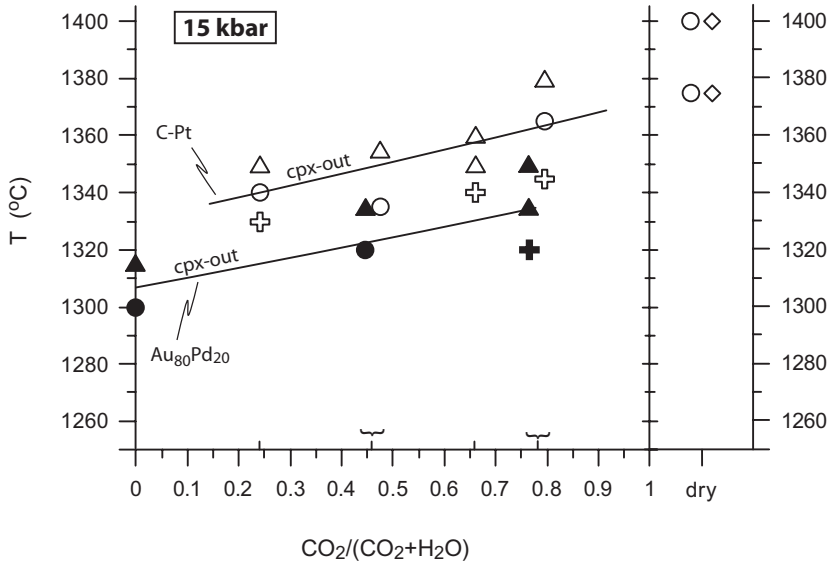

Fig. 5. Saturation experiments at 15 kbar. Open symbols, Pt–graphite double capsule; filled symbols, $Au_{80}Pd_{20}$ single capsule. Crosses, ankaramite layer partly crystallized to clinopyroxene, cpx + opx + ol + sp residue (corresponds to texture in Fig. 6a and b); circles, ankaramite layer fully molten, cpx + opx + ol + sp residue (Fig. 6c and d); triangles, opx + ol + sp residue (see Fig. 6e–g); diamonds, ol + cpx + sp residue. The experiments at $X_{CO_2} = 0{\cdot}46$ and 0·78 in C–Pt and AuPd capsules are slightly displaced in X_{CO_2} for clarity; this applies also to the dry experiments, in which different peridotite–ankaramite ratios resulted in different residual assemblages (see text).

At dry conditions, the volume mixing ratio for peridotite:ankaramite of 4:6 resulted in complete melting of orthopyroxene. Thus, the ankaramite melt was forced into saturation with opx + ol + sp in additional experiments, in which the mixing ratio was increased to 7:3. Even at 1400°C, we were not successful in saturating the resulting liquid in opx + ol + sp only, as clinopyroxene was still present. Nevertheless, the resulting melt (Table 5) in equilibrium with opx + cpx + ol + sp has a CaO/Al_2O_3 of 1·48 and a relatively low CaO content of 13·3 wt %.

In the normative olivine–diopside–quartz–CaTs + jadeite basalt tetrahedron (Yoder & Tilley, 1962; Green & Falloon, 1998) the experimental melts plot to normative diopside contents about twice those of previous determinations of melts from lherzolites or harzburgites (projected from olivine, Fig. 7). In projection from olivine, the experimental melts cover the field of parental melts from the Vanuatu arc. However, the latter have lower normative olivine contents, pointing towards significant olivine fractionation prior to eruption of the 'parental' melt compositions. In projection from diopside, our melts have higher normative olivine than experimental melts at comparable pressures in CO_2-free systems, reflecting a shift of the multiple saturation surface. A similar increase in olivine solubility at high CO_2 contents was previously observed for the olivine + orthopyroxene cotectic in the olivine–nepheline–quartz system (Taylor & Green, 1987) and in the olivine–kalsilite–quartz system (Edgar & Vukadinovic, 1992). This effect occurs also in complex natural basalts, in which the liquidus appearances of orthopyroxene, olivine, garnet and clinopyroxene shift as functions of CO_2 and H_2O contents (Brey & Green, 1977).

Residual phase compositions

Experimental phase compositions in equilibrium with ankaramitic melt are presented in Tables 5–7. Near the clinopyroxene-out reaction, all phases have high X_{Mg} values, olivines range from 0·90 to 0·94, orthopyroxenes from 0·91 to 0·95, and clinopyroxenes from 0·89 to 0·93. Ortho- and clinopyroxenes have low Al_2O_3 contents of 0·4–2·0 wt % and 0·9–2·9 wt %, respectively (all compositional values discussed in the text are for bulk compositions with $X_{Cr} = 0{\cdot}75$). Cr_2O_3 contents range from 0·8 to 1·7 wt % in orthopyroxenes and from 0·7 to 2·0 wt % in clinopyroxenes. Orthopyroxenes have Cr_2O_3 contents that are similar to or higher than Al_2O_3 contents (in wt %). Spinels are characterized by high chromium contents with an X_{Cr} value of 0·70–0·79 and have a small magnetite component (0·02–0·13 Fe^{3+} p.f.u.; see below).

The variation of phase compositions over the investigated temperature and X_{CO_2} range is small except for clinopyroxenes. Clinopyroxenes in equilibrium with orthopyroxene vary from 0·62 Ca p.f.u. at 1300°C to 0·36 Ca p.f.u. at 1340°C and to 0·21 Ca p.f.u. at 1380°C. In three experiments at temperatures from 1300 to 1330°C, three pyroxenes coexist: an orthopyroxene with ≤0·12 Ca p.f.u., a 'pigeonite' with 0·40–0·46 Ca p.f.u. and a 'high-Ca' clinopyroxene

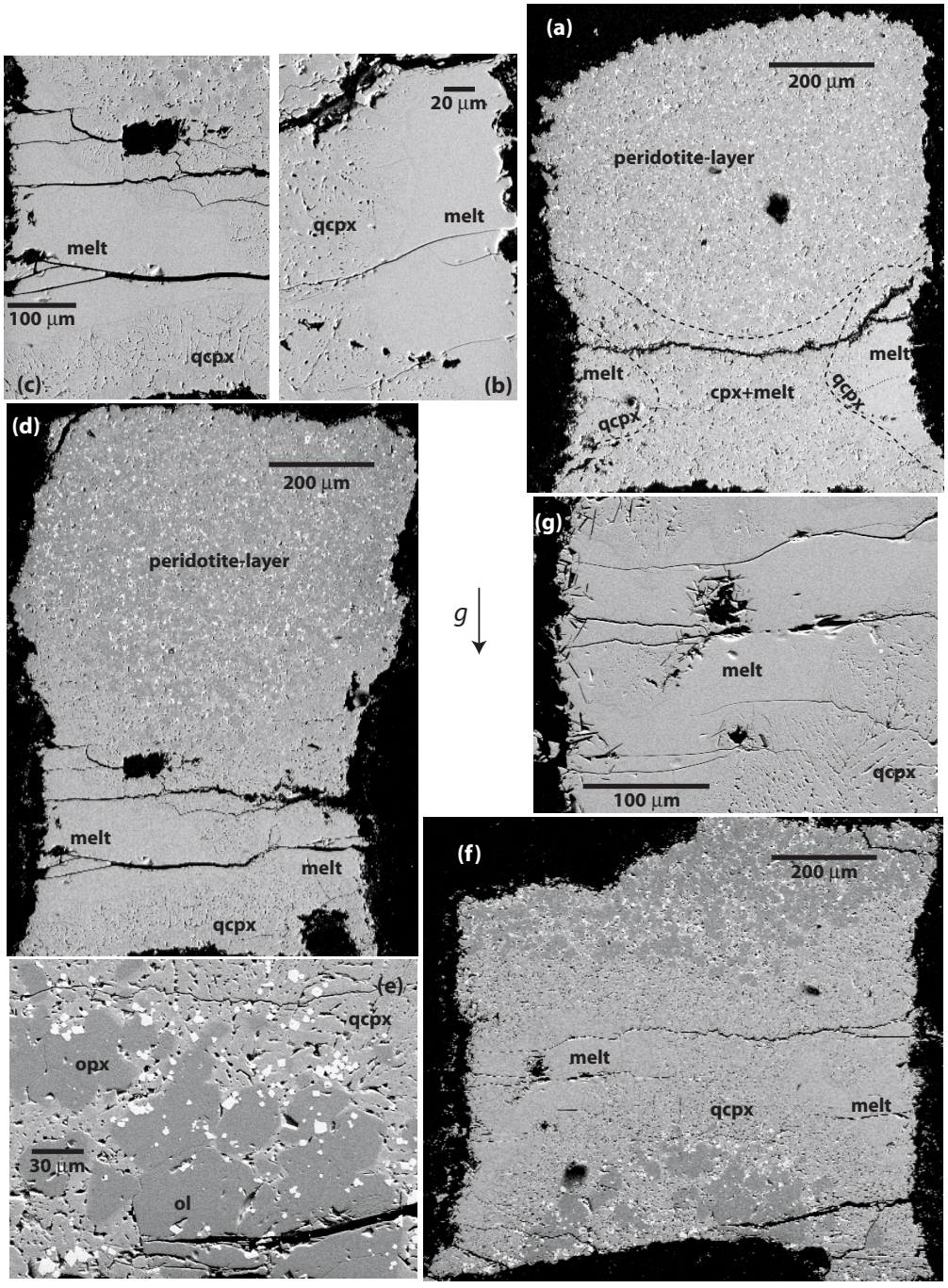

Fig. 6. BSE images of saturation experiments in graphite capsules. cpx, equilibrium clinopyroxene; qcpx, quench clinopyroxene; ol, olivine; opx, orthopyroxene. In all images, the bright phase is spinel; olivine and orthopyroxene are the dark grey phases. (a) D79, experiment with ankaramite layer partly crystallized to equilibrium clinopyroxene (labelled cpx + melt). Fully molten zone (now glass and quench-clinopyroxene) outlined to the right and left. The peridotite layer is composed of cpx + ol + opx + sp with little interstitial melt. (b) Detail of melt zone in the lower right of (a). (c, d) D80, characteristic texture of saturation experiment with fully molten ankaramite layer (i.e. now glass and quench-clinopyroxene), temperature just below the clinopyroxene-out reaction; cpx + opx + ol + sp in the peridotite layer. (c) Detail of melt-zone to the lower left of (d). The upper right corner displays the limit of the peridotite layer containing easily distinguishable dark grey ol + opx and bright spinel. (e–g) D81, typical texture of saturation experiment at temperature just above the clinopyroxene-out reaction. The peridotite layer with significantly coarser-grained orthopyroxene and olivine is reduced to about half of its initial thickness. Large orthopyroxene and olivine grains are present at the bottom of the capsule. (e) Detail of bottom opx + ol + sp layer. (g) Melt and quench-clinopyroxene, centre left of (f). It should be noted that at constant X_{CO_2}, the temperature difference between these three stages amounts to only 20–30°C.

Table 5: Experimental melt compositions from saturation experiments at 15 kbar

$CO_2/(H_2O + CO_2)$:	0	0·24	0·46	0·46	0·66	0·78	0·78	0·78	0·78	dry
Capsule:	AuPd	C–Pt	AuPd	C–Pt	C–Pt	AuPd	C–Pt	C–Pt peri-3	C–Pt peri-4	C–Pt
Run:	E8	E17	E4	D80		E30*	D82	E-28	F-16*	E7
T (°C):	1300	1340	1320	1335		1320	1365	1340	1360	1375
Residual pyroxene:	opx,cpx	opx,cpx	opx,cpx	opx,cpx		opx,cpx	opx,cpx	opx,cpx	opx,cpx	opx,cpx
n:	7	6	5	5		5	5	6	5	6
SiO_2	48·90	49·62	50·44	48·50		49·11	49·04	49·40	48·19	49·21
TiO_2	0·37	0·38	0·43	0·47		0·32	0·46	0·33	0·42	0·49
Cr_2O_3	0·36	0·66	0·49	0·52		0·52	0·79	0·05	0·33	0·71
Al_2O_3	11·26	9·00	10·61	10·16		11·04	8·80	10·07	11·45	10·07
FeO	8·10	9·05	6·02	9·75		8·18	9·43	9·41	9·92	9·42
MgO	15·79	16·59	16·46	15·89		15·00	16·98	15·96	14·84	15·99
CaO	13·59	13·50	13·94	13·13		13·73	13·14	13·41	13·51	12·64
Na_2O	1·21	0·89	1·21	1·19		1·38	1·01	1·04	0·93	1·19
K_2O	0·41	0·31	0·39	0·38		0·74	0·34	0·33	0·41	0·28
CaO/Al_2O_3	1·21	1·50	1·31	1·29		1·24	1·49	1·33	1·18	1·25
$X_{Mg}(Fe^{2+} = Fe^{tot})$	0·777	0·766	0·830	0·744		0·766	0·762	0·751	0·727	0·752
Fe^{3+}/Fe^{tot}*	0·107	0·041	0·060	0·031		0·062	0·030	0·017	0·041	0·008
X_{Mg}(olivine)	0·920	0·910	0·939	0·899		0·912	0·908	0·901	0·892	0·901
Run:	D90	D83	D89	D81	E16	E5	E6	E10	F31	G32
T (°C):	1315	1350	1335	1355	1350	1335	1380	1365	1380	1400
Residual pyroxene:	opx	opx	opx	opx	opx	opx	opx	opx	opx	cpx,opx
n:	5	14	5	6	4	5	6	5	8	7
SiO_2	50·47	49·93	49·74	49·35	49·21	49·32	49·84	50·19	49·42	49·13
TiO_2	0·38	0·34	0·35	0·37	0·40	0·41	0·33	0·23	0·36	0·47
Cr_2O_3	0·32	0·83	0·40	0·79	0·75	0·38	0·89	0·07	0·68	0·85
Al_2O_3	10·34	8·38	9·45	8·68	8·61	9·39	7·83	8·36	9·04	8·82
FeO	7·24	8·93	8·36	8·97	9·04	7·82	9·02	9·05	9·08	9·14
MgO	16·34	17·85	16·93	17·48	17·45	17·37	18·58	18·40	16·90	17·44
CaO	13·49	12·60	13·40	13·07	13·37	13·90	12·32	12·50	13·56	13·07
Na_2O	1·07	0·89	1·02	1·01	0·89	1·02	0·86	0·95	0·64	0·80
K_2O	0·35	0·26	0·34	0·27	0·28	0·38	0·25	0·24	0·31	0·27
CaO/Al_2O_3	1·31	1·50	1·42	1·51	1·55	1·48	1·57	1·50	1·50	1·48
$X_{Mg}(Fe^{2+} = Fe^{tot})$	0·801	0·781	0·783	0·776	0·775	0·798	0·786	0·780	0·768	0·773
Fe^{3+}/Fe^{tot}*	0·100	0·001	0·118	0·043	0·043	0·153	0·016	−0·015	−0·004	−0·021
X_{Mg}(olivine)	0·930	0·914	0·924	0·915	0·914	0·933	0·917	0·912	0·908	0·907

*Fe is recalculated into Fe^{3+} and Fe^{2+} to satisfy $Kd^{ol-liq}_{Fe^{2+}-Mg} = 0·337$ (at 15 kbar). A typical error including analytical uncertainties and sample inhomogeneity is ±0·020 in Fe^{3+}/Fe^{tot}. Analyses normalized to 100 wt %; n, number of analyses.

with ≥0·57 Ca p.f.u. The existence of two solvi at temperatures close to the stabilization of pigeonitic clinopyroxene is consistent with models derived from experiments on simple systems (Nickel & Brey, 1984). In our experiments, the Ca-rich solvus (i.e. the pigeonite–high-Ca clinopyroxene solvus) closes at 1340°C and at higher temperatures orthopyroxenes with roughly constant Ca of 0·10–0·11 a.p.f.u. coexist with 'pigeonites' that evolve from 0·36 Ca p.f.u. at 1340°C to 0·21 Ca p.f.u. at 1400°C.

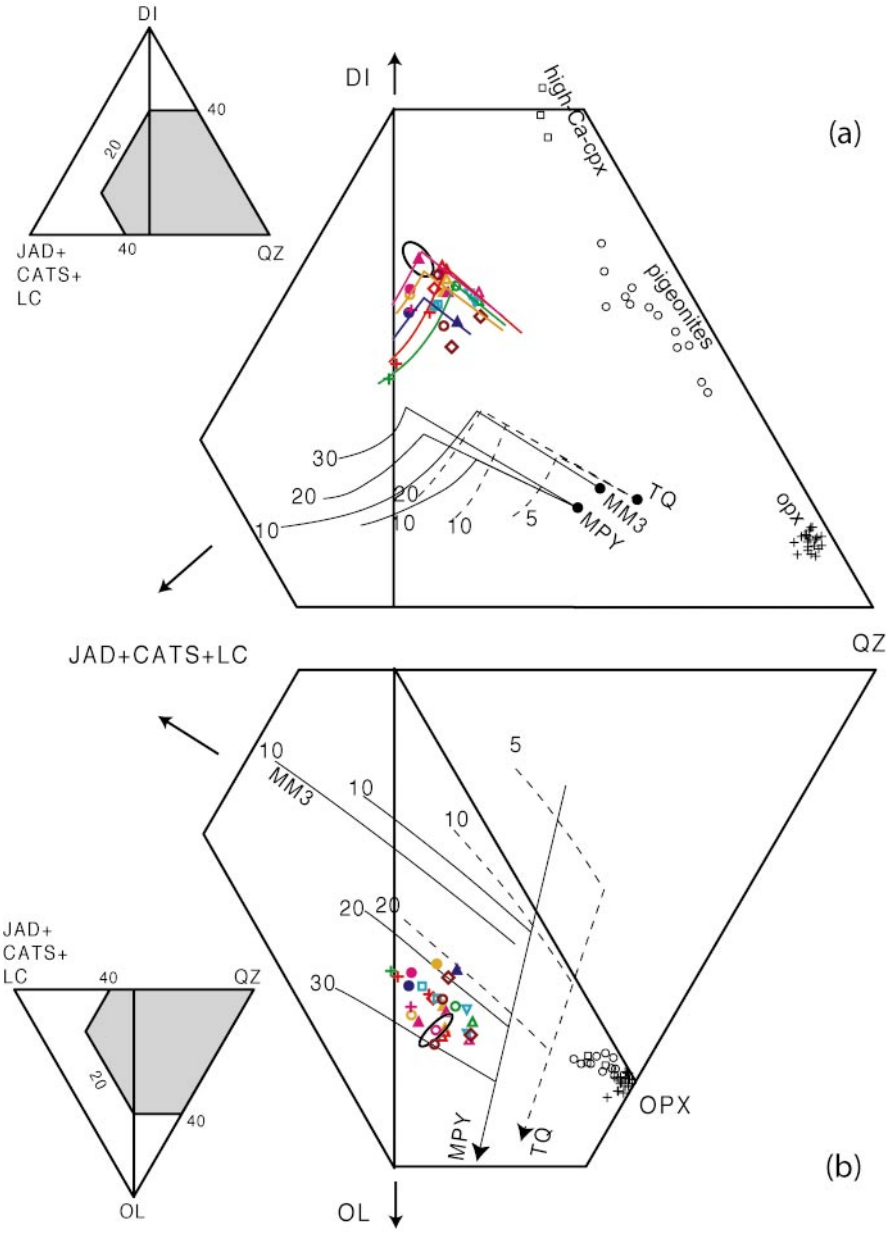

Fig. 7. (a) Di–Qz–(CaTs + Jad + Lc) face projected from olivine and (b) Ol–Qz–(CaTs + Jad + Lc) face projected from diopside. Experimental ultra-calcic melts and their melting lines compared with melting lines from lherzolites [MM3 from Hirschmann *et al.* (1998); MPY (MORB-pyrolite) and TQ (Tinaquillo lherzolite) from Falloon *et al.* (1988)]. Blue, $X_{CO_2} = 0{\cdot}0$; green, $X_{CO_2} = 0{\cdot}24$; orange, $X_{CO_2} = 0{\cdot}46$; red, $X_{CO_2} = 0{\cdot}66$; purple, $X_{CO_2} = 0{\cdot}78$; brown, dry; turquoise, $X_{CO_2} = 0{\cdot}78$ but different Cr/Al. Symbols as in Fig. 5. The ellipses represent a typical analytical error (in both projections, the error in SiO_2 has by far the largest contribution). Melting lines in (a) show the cpx + opx + ol cotectic lines followed by an abrupt change in direction when clinopyroxene is exhausted and melts evolve towards orthopyroxene. Experimental high-Ca clinopyroxenes (to maximum 1320°C), pigeonites and orthopyroxenes are shown. In the projection from diopside, the experimental 15 kbar melts are toward higher normative olivine contents than dry melts from the same pressure, higher X_{CO_2} causing generally higher normative ol contents. The relatively large scatter of melt compositions for each X_{CO_2} value is within analytical error.

Influence of capsule material and oxygen fugacity

Experiments with $Au_{80}Pd_{20}$ capsules yielded significantly higher Fe^{3+} contents in spinels (0·08–0·13 Fe^{3+} p.f.u.) than experiments with graphite–Pt double capsules (0·02–0·06, Fig. 8). K_D values for the Fe^{tot}–Mg distribution between melt and olivine are systematically lower than the equilibrium value of 0·337 at 15 kbar (Ulmer, 1989), and calculated Fe^{3+}/Fe^{tot} (Table 5, Fig. 8) in melts from graphite–Pt capsules are 0–4%, in contrast to 6–15% in melts from AuPd capsules (typical errors are ±2%). X_{Mg} values of minerals were 0·01–0·02 units higher in experiments

Table 6: Representative orthopyroxene, low-Ca pyroxene ('pigeonite'), and high-Ca pyroxene (subcalcic augite) analyses from saturation experiments at 15 kbar

Pyroxene:	opx	opx	opx	opx	pig	pig	pig	pig	Ca-cpx
Run:	E4	E17	D82	G32	E4	E17	D82	G32	E4
T (°C):	1320	1340	1365	1400	1320	1340	1365	1400	1320
Capsule:	AuPd	Pt–C	Pt–C	Pt–C	AuPd	Pt–C	Pt–C	Pt–C	AuPd
n:	11	17	9	5	8	6	11	3	21
				dry				dry	
SiO_2	56·86	56·97	56·13	56·25	55·15	55·67	54·29	55·86	54·24
TiO_2	0·07	0·05	0·02	0·03	0·06	0·05	0·08	0·04	0·06
Al_2O_3	0·59	1·36	1·30	1·62	2·44	1·54	1·97	1·33	1·68
Cr_2O_3	1·03	1·34	1·26	1·53	1·37	1·54	1·70	1·60	1·62
Fe_2O_3	0·62	0·09	0·40	0·40	0·00	0·00	0·41	0·34	0·24
FeO	3·70	5·53	5·24	4·98	3·76	5·00	4·69	5·14	2·92
MgO	33·86	33·13	32·43	32·80	25·55	27·09	25·88	29·41	22·51
CaO	2·75	2·65	2·86	2·83	11·37	9·44	10·08	6·74	15·73
Na_2O	0·12	0·06	0·12	0·05	0·27	0·21	0·29	0·14	0·39
K_2O	0·00	0·00	0·00	0·00	0·00	0·00	0·00	0·00	0·00
Total	99·6	101·2	99·8	100·5	100·0	100·6	99·4	100·6	99·4
Si	1·968	1·954	1·952	1·942	1·953	1·958	1·937	1·950	1·951
Ti	0·002	0·001	0·000	0·001	0·002	0·001	0·002	0·001	0·002
Al	0·024	0·055	0·057	0·066	0·102	0·064	0·083	0·055	0·071
Cr	0·028	0·036	0·036	0·042	0·038	0·043	0·048	0·044	0·046
Fe^{3+}	0·016	0·002	0·014	0·010	0·000	0·000	0·011	0·009	0·006
Fe^{2+}	0·107	0·159	0·150	0·143	0·111	0·147	0·140	0·150	0·088
Mg	1·745	1·691	1·682	1·688	1·345	1·416	1·374	1·530	1·204
Ca	0·102	0·098	0·103	0·105	0·431	0·356	0·386	0·252	0·606
Na	0·008	0·004	0·008	0·003	0·018	0·014	0·020	0·009	0·027
K	0·001	0·000	0·000	0·000	0·000	0·000	0·000	0·000	0·000
X_{Mg}	0·942	0·914	0·918	0·922	0·924	0·906	0·908	0·911	0·932
CaO/Al_2O_3	4·7	2·0	2·2	1·8	4·7	6·1	5·1	5·1	9·4

$X_{Mg} = Mg/(Mg + Fe^{2+})$. n, number of analyses.

with AuPd capsules compared with graphite capsules. Cr contents in melts from graphite capsules are almost twice those in melts from AuPd capsules, indicating a significant amount of Cr^{2+} in the former (Berry & O'Neill, 2000, and personal communication, 2001). Finally, the clinopyroxene-out reaction in the saturation experiments and the liquidus of the tested parental ankaramite are about 20°C lower in AuPd capsules compared with graphite capsules. These observations suggest that in graphite capsules, Fe was almost completely reduced to Fe^{2+} and Cr^{3+} was partly reduced to Cr^{2+}. In AuPd capsules, the initial oxidation state was approximately conserved (even without redox reactions, the initial Fe^{3+} fraction of 0·2 in the ankaramite layer is lowered by melting of solid phases that contain almost only ferrous iron) and the higher X_{Mg} values in the minerals are a consequence of higher Fe^{3+}/Fe^{tot} in the melt. The relative lowering of the phase boundaries could be explained by (1) more hydrogen in an oxidized compound (i.e. H_2O) in the $Au_{80}Pd_{20}$ capsules as compared with an increase of reduced compounds (i.e. CH_4) in the graphite capsules and (2) less hydrogen loss (and thus more H_2O dissolved in the melt) in the AuPd capsules as compared with C–Pt capsules. Finally, the observed differences between experiments in graphite–Pt double capsules and in $Au_{80}Pd_{20}$ single capsules is partly also due to the shorter run-times in the latter (2–4 h compared with 20·5–24 h in C–Pt), which imply less diffusive hydrogen loss through capsule walls.

Table 7: Spinel compositions in equilibrium with experimental ultra-calcic melts

Run:	E8	E17	E4	D80	E30	D82	F-16*	E7
Capsule:	AuPd	C–Pt	AuPd	C–Pt	AuPd	C–Pt	C–Pt	C–Pt
n:	5	8	4	3	7	3	—	4
SiO_2	0·58	0·29	0·48	0·26	0·38	0·25		0·54
TiO_2	0·36	0·25	0·50	0·23	0·33	0·25		0·37
Al_2O_3	11·05	14·32	11·43	17·59	15·23	14·25		15·01
Cr_2O_3	57·25	56·12	60·05	52·20	51·02	55·70		55·00
Fe_2O_3	4·47	1·55	2·11	1·98	6·15	1·86		2·08
FeO	10·57	11·03	9·15	11·23	11·33	10·55		11·02
MgO	15·21	14·94	16·47	14·90	15·12	14·83		15·26
CaO	0·31	0·27	0·31	0·25	0·32	0·24		0·22
Total	99·8	98·8	100·5	98·6	99·9	97·9		99·5
Si	0·018	0·009	0·015	0·008	0·012	0·008		0·017
Ti	0·009	0·006	0·012	0·006	0·008	0·006		0·009
Al	0·413	0·533	0·420	0·647	0·560	0·535		0·552
Cr	1·434	1·403	1·481	1·288	1·258	1·402		1·356
Fe^{3+}	0·107	0·037	0·050	0·046	0·144	0·045		0·049
Fe^{2+}	0·280	0·291	0·239	0·293	0·295	0·281		0·287
Mg	0·718	0·703	0·766	0·693	0·703	0·703		0·710
Ca	0·011	0·009	0·011	0·009	0·011	0·008		0·007
X_{Mg}	0·719	0·707	0·762	0·703	0·704	0·714		0·712
X_{Cr}	0·776	0·725	0·779	0·666	0·692	0·724		0·711

Run:	D90	D83	D89	D81	E16	E5	E6	F31*	G32
Capsule:	AuPd	C–Pt	AuPd	C–Pt	C–Pt	AuPd	C–Pt	C–Pt	C–Pt
n:	6	6	12	10	3	3	5	3	
SiO_2	0·50	0·34	0·42	0·25	0·31	0·29	0·36	0·07	0·00
TiO_2	0·51	0·17	0·48	0·25	0·10	0·64	0·14	0·19	0·22
Al_2O_3	11·47	12·80	10·09	13·57	12·31	15·00	11·32	14·78	14·81
Cr_2O_3	56·70	58·88	56·11	57·61	58·49	51·91	60·55	56·74	56·46
Fe_2O_3	3·37	1·23	5·25	1·00	2·48	5·56	1·11	2·11	2·29
FeO	9·65	10·76	10·42	10·97	10·47	8·15	10·70	10·38	10·12
MgO	15·76	15·25	14·94	15·03	15·07	16·70	14·86	15·75	15·82
CaO	0·29	0·22	0·30	0·27	0·29	0·27	0·29	0·18	0·19
Total	98·3	99·7	98·0	99·0	99·5	98·5	99·3	100·2	99·9
Si	0·016	0·011	0·014	0·008	0·010	0·009	0·011	0·002	0·000
Ti	0·012	0·004	0·012	0·006	0·003	0·015	0·003	0·004	0·005
Al	0·433	0·476	0·386	0·507	0·459	0·552	0·425	0·542	0·544
Cr	1·434	1·469	1·440	1·444	1·464	1·282	1·526	1·396	1·392
Fe^{3+}	0·081	0·029	0·128	0·024	0·059	0·131	0·027	0·049	0·054
Fe^{2+}	0·258	0·284	0·283	0·291	0·277	0·213	0·285	0·270	0·264
Mg	0·752	0·717	0·723	0·710	0·711	0·777	0·706	0·730	0·735
Ca	0·010	0·008	0·011	0·009	0·010	0·009	0·010	0·006	0·006
X_{Mg}	0·745	0·716	0·719	0·709	0·720	0·785	0·712	0·730	0·736
X_{Cr}	0·768	0·755	0·789	0·740	0·761	0·699	0·782	0·720	0·719

$X_{Mg} = Mg/(Mg + Fe^{2+})$. $X_{Cr} = Cr/(Cr + Al)$. *n*, number of analyses.
*Low bulk X_{Cr} of 0·466; in F16, spinels were too small to be measured by microprobe.

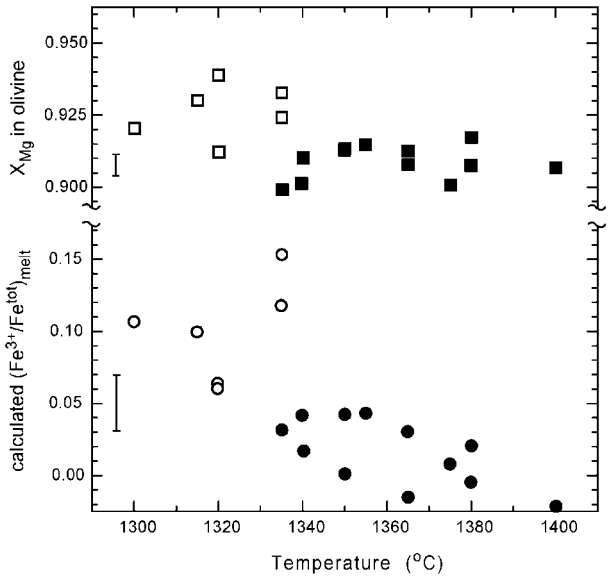

Fig. 8. Calculated Fe^{3+}/Fe^{tot} ratios in melt and measured X_{Mg} values in olivine. Fe^{3+} is calculated from Mg/Fe^{2+} partitioning between olivine and melt. Open symbols, $Au_{80}Pd_{20}$ single capsules; filled symbols, C–Pt double capsules. Typical error bars for both ratios are given at the left-hand side. Experiments in $Au_{80}Pd_{20}$ capsules result in significantly higher $X_{Mg}^{olivine}$ and Fe^{3+} fractions in melt than experiments in Pt–C capsules.

CaO/Al_2O_3 values in the experimental melts differ for AuPd and C–Pt capsules in that the former have ratios that are *c.* 0·1 units lower. MgO contents are also slightly lower in experiments from AuPd capsules. Whether the reason for this difference is in the difference of oxidation state, the probably higher H_2O contents in the melts from AuPd capsules, and/or in a different speciation of volatile components will be the subjects of further investigation. Whereas the oxidation state in the C–Pt capsules is probably appropriate for average mantle, the somewhat oxidized mantle wedge above subduction zones might be better represented by the experimental configuration with $Au_{80}Pd_{20}$ capsules.

DISCUSSION

Genesis of the Epi ankaramite suite

The most significant difference between the experimental ultra-calcic melts and the Epi parental melt is the significantly higher MgO contents in the experimental melts. Fractionation of olivine would conserve the high CaO/Al_2O_3 values, increase CaO (and Al_2O_3) contents and decrease MgO contents and X_{Mg} values of the liquid. Fractionation models were tested for olivine, clinopyroxene and Cr-spinel/magnetite starting from various experimental melt compositions. Experimental melts with residual clinopyroxene yielded fits with an R^2 of 0·2–1·2, but those without clinopyroxene in the residue did not reproduce the Epi ankaramite parental magma ($R^2 > 2·5$). The fit results (two examples in Table 8) show the following:

(1) starting from the relatively reduced experimental melts from Pt–C capsules, and from melt compositions formed at low to moderate X_{CO_2}, fractionation of 4–6 wt % olivine and about 1 wt % of magnetite produces melts of the Epi parent composition. If clinopyroxene fractionation or accumulation is allowed for, fit residuals do not significantly improve, resulting in 1–2 wt % clinopyroxene accumulation.

(2) Starting from the less reduced melts from AuPd capsules, fractionation of 4–6 wt % olivine and accumulation of 3–4 wt % magnetite result in melts close to the Epi parent composition. When allowing for clinopyroxene variation, accumulation of 3–5 wt % does improve the fit quality slightly.

(3) Some Cr-spinel fractionation would be necessary to account for the difference in Cr_2O_3 concentration between experimental melts and the parental Epi magma. However, the small excess of Cr in the experimental melts rather reflects fairly reducing conditions in the experiments than natural conditions and is thus regarded as an 'experimental artefact'.

The fractionation of olivine during magma ascent is expected for melts with dissolved CO_2 and H_2O, high MgO and high normative olivine contents. When the magma ascends from 15 or 20 kbar, CO_2 solubility in the magma decreases markedly around 10 kbar. As a consequence, C–H–O fluid dominated by CO_2 is degassed. The olivine saturation surface therefore moves towards lower MgO and normative olivine contents, and olivine is precipitated at the fluid-saturated liquidus (e.g. Taylor & Green, 1987; Edgar & Vukadinovic, 1992).

The mass balance calculations, which relate our experimental melts to the Epi parent, yield good fits within the uncertainty of choices of both the parental Epi magma and the refractory peridotite residue. We consider that our experimental melts at low to moderate X_{CO_2} fractions are suitable parents for the ankaramite suites in the Vanuatu arc. The major implication is that primitive parents to the Vanuatu arc ankaramite suites were not ultra-calcic melts in terms of CaO contents, but melts high in MgO and CaO/Al_2O_3. Subsequent fractionation of olivine, as a result of pressure decrease and degassing of CO_2, has increased CaO concentrations to values at which clinopyroxene precipitation reverses this trend (Barsdell, 1988; Barsdell & Berry, 1990; Eggins, 1993). The CaO/Al_2O_3 values observed in the ankaramites of the Vanuatu arc are not extreme in terms of our experimental range and lie at the lower end of the experimentally obtained melts.

Table 8: Mass balance for fractionating experimental melts into the Epi parent magma

wt %	D80 melt	Fractionation result starting from D80 melt					E4 melt	Fractionation result starting from E4 melt				
		ol*	Cr-sp*	cpx†	mgt†	Epi-parent		ol*	Cr-sp*	cpx†	mgt†	Epi-parent
SiO_2	48·50	40·64	0·26	54·40	0·00	49·07	50·44	41·79	0·00	54·40	0·00	49·07
TiO_2	0·47	0·00	0·23	0·00	0·81	0·38	0·43	0·00	0·50	0·00	0·81	0·38
Cr_2O_3	0·52	0·00	52·20	0·77	0·00	0·08	0·49	0·14	60·05	0·77	0·00	0·08
Al_2O_3	10·16	0·00	17·59	0·85	11·50	11·00	10·61	0·00	11·43	0·85	11·50	11·00
FeO	9·75	10·05	11·23	2·02	73·90	8·72	6·02	6·24	11·05	2·02	73·90	8·72
MgO	15·89	48·82	14·90	18·20	7·80	14·53	16·46	51·43	16·47	18·20	7·80	14·53
CaO	13·13	0·34	0·25	23·80	0·00	14·78	13·94	0·26	0·00	23·80	0·00	14·78
Na_2O	1·19	0·00	0·00	0·00	0·00	1·08	1·21	0·00	0·00	0·00	0·00	1·08
K_2O	0·38	0·00	0·00	0·00	0·00	0·29	0·39	0·00	0·00	0·00	0·00	0·29
CaO/Al_2O_3	1·29	—	0·01	28·0	0·00	1·34	1·31	—	1·30	28·0	0·00	1·34
X_{Mg}‡	0·744	0·896	0·703	0·941	0·158	0·748	0·830	0·896	0·903	0·941	0·158	0·748
ol–Crsp–cpx–mgt	$R^2 = 1·15$	4·9	0·0	−2·0	0·9	96·2	$R^2 = 0·19$	5·1	0·5	−4·4	−4·2	103·0
ol–Crsp–mgt	$R^2 = 1·18$	4·7	0·1	—	1·2	94·0	$R^2 = 0·49$	4·7	0·7	—	−3·7	98·3
ol–mgt	$R^2 = 1·20$	4·7	—	—	1·2	94·1	$R^2 = 0·37$	5·3	—	−4·6	−4·2	103·5
ol–cpx–mgt	$R^2 = 1·14$	4·9	—	−1·9	0·9	96·1	$R^2 = 0·69$	4·9	—	—	−3·6	98·6

Two experimental melts (D80—relatively reduced, Pt–graphite capsule; E4—relatively less reduced, AuPd capsule) are fitted to mineral phases in equilibrium either with the source (olivine, Cr-spinel) or with the Epi-parent (high-Ca cpx, magnetite) and to the Epi-parent. This calculation results into fractionated or accumulated mineral fractions necessary to produce the Epi-parent from the experimental melts. The last four lines give fit results as modal amounts in wt % and fit quality (R^2) allowing for four, three or two minerals plus the Epi-parent fitted to the experimental melts. Spinels have low totals as all Fe is Fe^{2+} in this mass balance calculation.
*Mineral compositions from experiments.
†Mineral compositions from most primitive Epi-lava.
‡$X_{Mg} = Mg/(Mg + Fe^{tot})$.

A model source (and residue) for hypersthene-normative ankaramitic magmas *or* tuning the CaO/Al_2O_3 ratio of the source

The compositions of minerals equilibrated with the experimental ultra-calcic melts are characteristic for refractory harzburgitic mantle. Low Al_2O_3 in ortho- and clinopyroxene and low Na_2O contents in clinopyroxene (if residual) are consistent with a mantle that underwent prior melt extraction; high X_{Cr} in spinels is also typical of refractory mantle. Our experiments do not constrain the modal composition of the source and thus we calculate a suitable source.

The most favourable way to generate high CaO/Al_2O_3 residues from first-stage melting of fertile lherzolite is to extract a moderate amount (6–18%) of melt with low CaO/Al_2O_3. Melts of this character are typical of low pressures and are derived from plagioclase lherzolite. A likely source (and residue) for ultra-calcic melts is exemplified in Table 9. We calculated possible residues after a first-stage melt extraction by subtracting published experimental melt compositions for well-studied mantle compositions (Hawaiian Pyrolite, HPy, Jaques & Green, 1980; Falloon *et al.*, 1988; MM3, Baker & Stolper, 1994; Hirschmann *et al.*, 1998; KLB-1, Hirose & Kushiro, 1993; garnet lherzolite PHN1611, Kushiro, 1996; Tinaquillo Lherzolite, Tql, Jaques & Green, 1980; Falloon *et al.*, 1988, 1999) employing reported melt fractions that leave at least a few percent clinopyroxene in this first-stage residue (Fig. 9). Although we recognize that there are some problems in some experimental datasets of liquid composition and reacting bulk composition [as illustrated in Fig. 2 and discussed by Hirschmann *et al.* (1998) and Falloon *et al.* (1999)], a clear picture emerges from Fig. 9. Subtracting relatively low-pressure melts from fertile lherzolites leads to a strong increase of CaO/Al_2O_3 in the residue. The CaO/Al_2O_3 values of the resulting, somewhat refractory mantle would range from 1·2 to 1·8 for the respective compositions MM3, Tql, HPy and KLB-1, and to even higher values for PHN1611. These ratios are achieved by batch melting; fractional melting would increase the resulting CaO/Al_2O_3 as, at

Table 9: Mass balance for melting processes leading from fertile mantle to the Epi ankaramite parent magma

	HPy	Melt 5 kbar 1200°C	Refractory source RS HPy − 17·5% m5k	E16, 1350°C, $X_{CO_2} = 0{\cdot}66$				Residue = RS − 10·9% E16-melt	D80, 1335°C, $X_{CO_2} = 0{\cdot}46$					Residue = RS − 4·2% D80-melt
				ol	opx	melt	sp		ol	opx	cpx	melt	sp	
				75·0%*	13·8%	10·6%	0·7%		74·9%	16·8%	3·8%	4·2%	0·4%	
SiO_2	45·4	52·1	43·95	41·27	56·71	49·21	0·31	43·33	40·64	55·93	53·92	48·50	0·26	43·69
TiO_2	0·7	3·0	0·23	0·00	0·05	0·40	0·10	0·01	0·00	0·09	0·07	0·47	0·23	0·02
Cr_2O_3	0·4	—	0·46	0·35	1·20	0·75	58·63	0·94	0·00	1·32	1·77	0·52	52·20	0·52
Al_2O_3	3·6	14·9	1·14	0·00	1·02	8·61	12·34	0·25	0·00	2·03	2·49	10·16	17·59	0·53
FeO	8·5	7·8	8·60	8·31	5·26	9·04	12·73	7·87	10·05	6·20	5·08	9·75	11·23	9·19
MgO	37·7	8·9	43·78	49·79	33·18	17·45	15·11	46·96	48·82	32·24	23·94	15·89	14·90	44·80
CaO	3·1	9·5	1·73	0·29	2·48	13·37	0·29	0·63	0·34	2·64	12·30	13·13	0·25	1·22
Na_2O	0·6	2·8	0·10	0·00	0·09	0·89	0·00	0·01	0·00	0·15	0·31	1·19	0·00	0·04
K_2O	0·1	0·6	0·03	0·00	0·00	0·28	0·00	0·00	0·00	0·00	0·00	0·38	0·00	0·00
CaO/Al_2O_3	0·87	0·64	1·52	—	2·43	1·55	0·02	3·21	—	1·30	4·94	1·29	0·01	2·30
X_{Mg}	0·888	0·670	0·901	0·914	0·918	0·775	0·679	0·914	0·896	0·903	0·894	0·744	0·703	0·897
Ol*	54·0		73·0					84·9						78·2
Opx	28·0		18·6					14·8						17·5
Cpx	12·8		7·6					—						4·0
Plag	3·9		—					—						—
Sp	1·3		0·8					0·3						0·4
				fit to RS: $R^2 = 0{\cdot}52$					fit to RS: $R^2 = 0{\cdot}47$					

The refractory source RS is calculated from Hawaian Pyrolite extracting an amount of melt (less than the observed amount of 20%) that results in the most suitable source for the subsequent calculations. Melt composition from 5 kbar, 1200°C (Jaques & Green, 1980; Falloon *et al.*, 1988). This refractory mantle source 'RS' is then fitted to the observed phases in experiments E16 (opx–ol–sp residue, cpx exhausted) and D80 (cpx–opx–ol–sp residue). The amount of melt from this calculation is then subtracted from 'RS' and yields the two refractory residues.

*All fit results and modes in wt %.

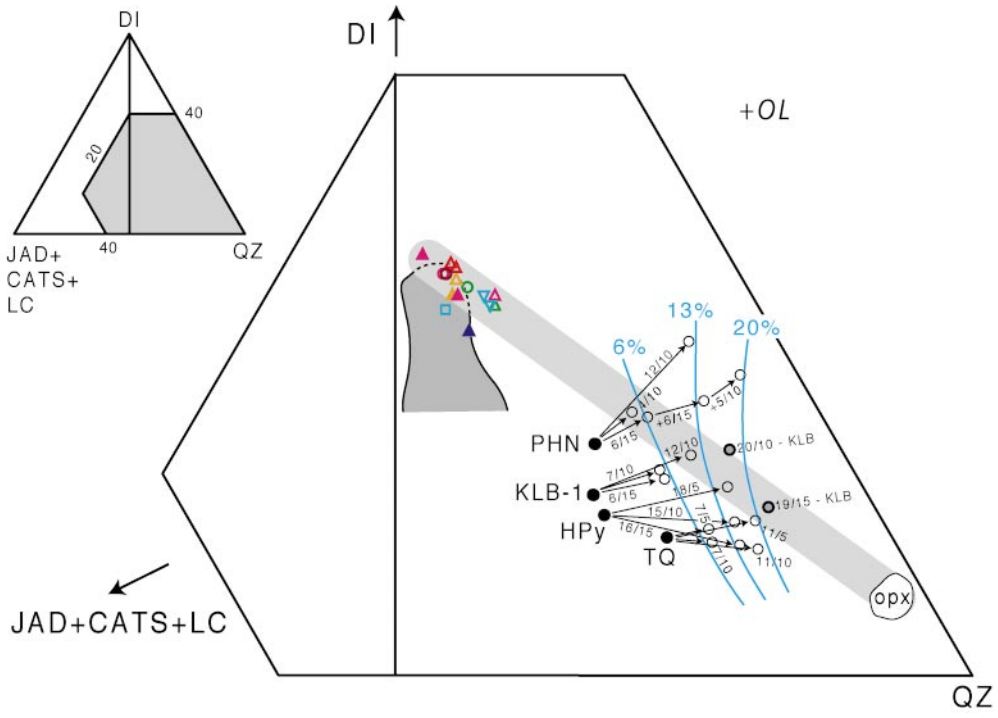

Fig. 9. Di–Qz–(CaTs + Jad + Lc) face of the modified basalt octahedron, projected from olivine. The experimental ultra-calcic melts (coloured symbols; for coding see Fig. 7) saturated in orthopyroxene + olivine may be formed from any refractory source projecting between orthopyroxene and the ultra-calcic melts (light grey array). Field labelled 'opx' indicates experimental orthopyroxene compositions of this study. First-stage melt extraction displaces residual peridotites as indicated by arrows. Labels are melt fraction/experimental pressure; the sequence of three arrows indicates fractional melt extraction (Hirose & Kushiro, 1998). Blue lines, contours for extracted melt percentage. The most fertile peridotites are towards the diopside apex and, as any low-pressure melt plots towards lower normative diopside, residues move towards higher CaO/Al_2O_3. The dark grey field corresponds to the natural hypersthene-normative ultra-calcic melts except for those from the Lau basin (compare with Fig. 1).

the relevant conditions, Al_2O_3 partitions more strongly into the melt than CaO (Hirose & Kushiro, 1993). Phase assemblages (ol + opx + cpx + sp + melt or ol + opx + sp + melt) from our experiments were then fitted to the first-stage residues. The best fit of our experimental phase compositions was obtained for the residue RS, which has a CaO/Al_2O_3 of 1·52, and results from Hawaiian Pyrolite with a 5 kbar, 1200°C melt (F = 17·5%, Jaques & Green, 1980; Falloon *et al.*, 1988) extracted. Second-stage melting of this residue yields melt fractions of 4–5% for melts with CaO/Al_2O_3 near 1·3 and an olivine–orthopyroxene–clinopyroxene–spinel residue. Complete melting of clinopyroxene in the refractory source RS occurs at F = 10–12% for melts with CaO/Al_2O_3 near 1·5 (Table 9).

The evolution of melt compositions in experimental studies on fertile mantle is illustrated in Figs 1 and 2. In each study, maximum CaO/Al_2O_3 in melts is reached at the elimination of residual clinopyroxene and melts then evolve with near-constant or decreasing CaO/Al_2O_3 (Fig. 2) along the olivine + orthopyroxene + spinel cotectic. In projection from olivine, this cotectic represents an almost straight line into the orthopyroxene compositional field (Figs 7 and 9). Source compositions and their derivative melts in equilibrium with harzburgite residue lie along this line passing through the bulk composition and the composition of residual orthopyroxene (Figs 1 and 7). This line defines the maximum CaO/Al_2O_3 for partial melts from a particular composition; liquids with lherzolite residue lie below the prolongation of this line (i.e. away from the Di apex). Thus, in projection from olivine, a mantle source composition for ultra-calcic melts must lie on or at higher normative diopside contents than a line from orthopyroxene to the experimental melt compositions. The X_{Cr} of the source composition must be greater than those of experimental fertile compositions (e.g. HPy, MPy, MM3, KLB-1, PHN1611) so that residual spinel at clinopyroxene elimination has $X_{Cr} > 0{\cdot}7$.

If only melt extraction is considered as a means of 'tuning' the source composition, then modal clinopyroxene must be low in suitable sources, i.e. typically between 2 and 6 wt %, and complete melting of clinopyroxene requires melt fractions only slightly larger. When melting occurs up to the clinopyroxene-out curve, melt compositions necessarily inherit a CaO/Al_2O_3 close to the bulk CaO/Al_2O_3 and melts acquire the complete inventory of the more incompatible

elements previously concentrated in clinopyroxene. Residual spinel will increase CaO/Al_2O_3 in the melt slightly and the most extreme ratios might be obtained at small melt fractions and high Cr_2O_3 content in the residue (and thus high amounts of Cr-rich spinels). In the model under discussion, the highest possible CaO/Al_2O_3 in a melt depends on the amount and mode of previous melt extraction from the mantle source.

In Fig. 9, we calculate a range of such melt extraction models, seeking to generate residues that lie on or above the line joining residual orthopyroxene and the ultra-calcic melts (e.g. the Epi parent magma). The figure demonstrates that appropriate residues are achieved if the initial fertile lherzolite already has relatively high normative diopside and CaO/Al_2O_3. Appropriate residues with sufficiently high CaO/Al_2O_3 and X_{Cr} from mantle with subchondritic or chondritic CaO/Al_2O_3 values are difficult to reach.

Previous experiments on the genesis of melts with high CaO/Al_2O_3

Our experimental methods have established that island-arc ankaramites characterized by CaO/Al_2O_3 up to $\sim$1·5 do not require an orthopyroxene-absent wehrlitic or pyroxenitic source but can be derived from a lherzolitic source, leaving residual refractory clinopyroxene-bearing or clinopyroxene-free harzburgite. Conditions near 15 kbar and temperatures of 1300–1360°C are appropriate in the presence of some dissolved CO_2 and H_2O, which lower the liquidus temperatures. In dry systems, temperatures of 1400°C are necessary to produce ultra-calcic melts with a CaO/Al_2O_3 of 1·5 from refractory lherzolite.

As an alternative to a refractory mantle source, ultra-calcic melts were also produced by melting of wehrlitic sources at high melt fractions (Pickering-Witter & Johnston, 2000; Kogiso & Hirschmann, 2001; Schwab & Johnston, 2001; see Fig. 10). In fact, any wehrlitic source must produce melts that will, with high degrees of melting, move towards the diopside apex in Fig. 10 and have a maximum CaO/Al_2O_3 close to the clinopyroxene composition in the starting material. The composition of the first melt to form from a given wehrlite depends on the exact composition of the clinopyroxene in a two-phase starting material or on the exact composition of clinopyroxene + minor phases (spinel, small amounts of orthopyroxene) in a multi-phase starting material. In the study of Kogiso & Hirschmann (2001), the absence of orthopyroxene in combination with moderate amounts of Na_2O and Al_2O_3 in the clinopyroxene (e.g. 0·8 and 5·6 wt %, respectively) resulted in nepheline-normative melts (Fig. 10). Melts with $CaO/Al_2O_3 > 1·1$ are reached near 1350°C at melt fractions around 30%. Pickering-Witter & Johnston (2000) and Schwab & Johnston (2001) both studied the melting systematics of modally variable peridotites. In both studies, one wehrlitic starting material contained 7 wt % orthopyroxene, which immediately melted out (and is partly accommodated as clinoenstatite component in clinopyroxene). Nevertheless, the presence of orthopyroxene in the starting material shifted initial melt compositions towards the Opx/Qz apex in Fig. 10. The 7 wt % orthopyroxene combined with a clinopyroxene containing 1·5 and 6·4 wt % Na_2O and Al_2O, respectively, results in a melting trend towards the diopside apex, which is slightly nepheline-normative (FER-B, Pickering-Witter & Johnston, 2000), and ultra-calcic melts occur near 1350°C at melt fractions around 30%. Combination of 7 wt % orthopyroxene with a refractory clinopyroxene having 0·5 and 3·1 wt % Na_2O and Al_2O (INT-B, Schwab & Johnston, 2001) results in hypersthene-normative melts, which become ultra-calcic near 1350°C at melt fractions of 10–15%, melts with CaO/Al_2O_3 near 1·5 are reached at 1380°C and melt fractions of 20%. Finally, it should be pointed out that this starting material (INT-B, ol:opx:cpx:sp = 50:7:40:3) is made of refractory mantle phases. As a result of the high normative orthopyroxene content in the first melt of this material, its melting trajectory, projected from olivine, passes through the projection points representing our experimental melt compositions.

All of the experimental studies on wehrlite sources produced ultra-calcic melts. This is a mere consequence of the starting compositions, which have little or no orthopyroxene and CaO/Al_2O_3 ranging from 1·7 to 3·4. Melt compositions evolve along the olivine + clinopyroxene cotectic (Fig. 10) towards the bulk CaO/Al_2O_3 at high melt fractions. However, only the melt compositions of Schwab & Johnston (2001) at melt fractions near 20% are suitable parents for hypersthene-normative melts. Their starting material is wehrlitic, but contains refractory orthopyroxene and clinopyroxene and has a CaO/Al_2O_3 of 3·4.

Nepheline-normative ultra-calcic melts

As pointed out above, ultra-calcic melts can be subdivided into a hypersthene- and a nepheline-normative group (Schiano *et al.*, 2000; Kogiso & Hirschmann, 2001), the former including the Epi suite. The nepheline-normative suite, which occurs only in the arc setting, has not only low SiO_2 and high total alkalis, but also lower MgO contents, higher CaO and Al_2O_3, and lower CaO/Al_2O_3 than the hypersthene-normative group. X_{Mg} values of nepheline-normative ultra-calcic magmas are generally less than 0·72

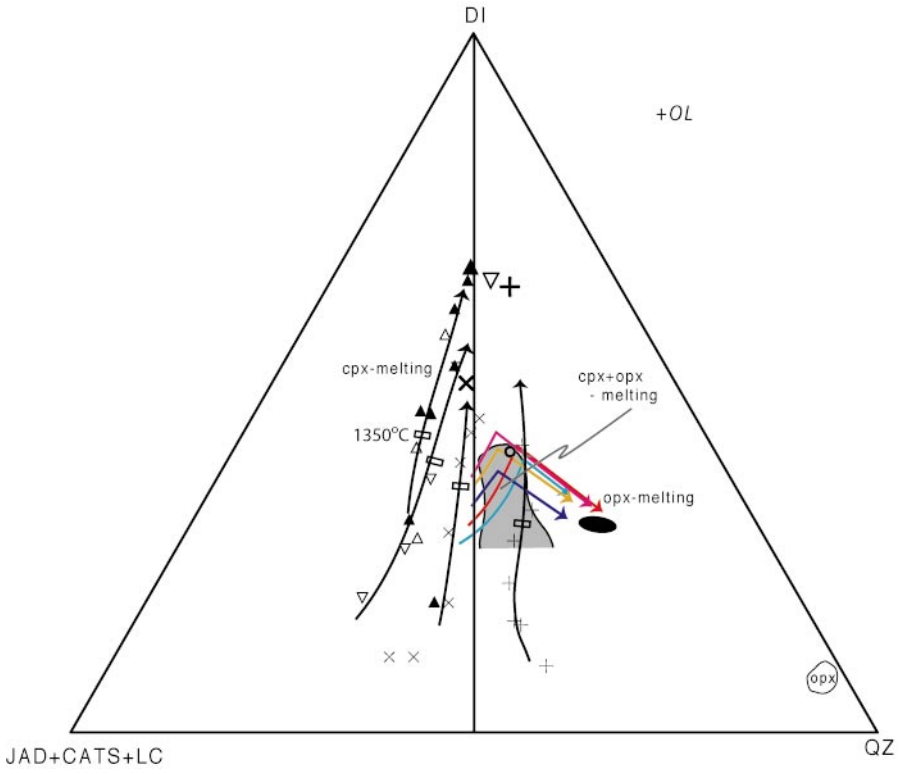

Fig. 10. Comparison of experimentally produced ultra-calcic melts and starting materials on the Di–Qz–(CaTs + Jad + Lc) face of the modified basalt octahedron, projected from olivine. Triangles, Kogiso & Hirschmann (2001) (▲, OLCPX1; △, OLCPX2; ▽, Pyrox2B). ×, FER-B, Pickering-Witter & Johnston (2000); +, INT-B, Schwab & Johnston (2001). Large symbols represent the starting materials, small symbols experimental melt compositions. Coloured lines indicate melting trends of this study, colour coded for different X_{CO_2} (see Fig. 7); ○, dry melt saturated in opx + cpx + ol + sp; field labelled 'opx' indicates experimental orthopyroxene compositions of this study. Black ellipse, bulk compositions of this study; the scatter corresponds to slightly different ankaramite:peridotite layer ratios in individual experiments. The black arrows correspond to melting trends in wehrlites and represent projection of the ol + cpx cotectic. The coloured arrows from this study first follow an ol + cpx + opx cotectic and after exhaustion of cpx (change in direction) an ol + opx cotectic. The open rectangle on each line corresponds to an experimental temperature of 1350°C; all melts except those represented by the two uppermost ▽ symbols are olivine-saturated.

whereas hypersthene-normative ultra-calcic magmas range to 0·79.

Generally, the alkali-rich character of the nepheline-normative suite is incompatible with the refractory nature of our proposed source. The low SiO_2 contents of the nepheline-normative melts are also incompatible with saturation in orthopyroxene. In addition, the X_{Mg} values of the nepheline-normative suite preclude equilibration with refractory mantle minerals. The nepheline-normative suite is limited to the arc environment and it is possible that slab-derived fluids add alkalis to the source region. However, such fluids are not only Na_2O- and K_2O-rich but also SiO_2-rich and thus are unsuitable for generating low-SiO_2 magmas. We thus suggest that the group of nepheline-normative ultra-calcic melts is generated through a process different from second-stage melting of refractory mantle. A suitable source could involve significant addition of a mobile component (fluid or carbonatite melt) and metasomatic phases (e.g. amphibole or/and phlogopite), or a possibly wehrlitic cumulate (with significantly lower X_{Mg} than refractory mantle) different from clinopyroxene-bearing refractory mantle, or a combination of both (Medard *et al.*, 2002).

A model for hypersthene-normative ultra-calcic melts

In the model discussed, hypersthene-normative ultra-calcic melts are produced from refractory lherzolite mantle at low melt fractions. In any major magmatic environment, i.e. in mid-ocean ridge, arc and ocean-island settings, refractory mantle is readily available. The highest bulk CaO/Al_2O_3, and thus the most suitable preconditioning of the mantle with respect to generation of ultra-calcic magmas, would occur in a refractory mantle containing small amounts of clinopyroxene. The most extreme ultra-calcic melts would

represent melt fractions of less than a few percent from this latter source. In the volatile-bearing experiments we have arbitrarily used a bulk composition with $CaO/Al_2O_3 = 1{\cdot}35–1{\cdot}39$, yielding melt compositions with CaO/Al_2O_3 up to 1·57. In our dry experiments, the bulk CaO/Al_2O_3 was varied from 1·35 to 1·80, yielding melts with a maximum CaO/Al_2O_3 of 1·48. The latter melts still coexist with cpx + opx + ol + sp. This study does not cover the entire range of CaO/Al_2O_3 values observed, i.e. it does not include the melt inclusions from the Lau back-arc basin (Kamenetsky *et al*. 1997). However, extreme CaO/Al_2O_3 values could be reached by fractional melting: extraction of 10% first-stage melt from fertile mantle (CaO/Al_2O_3 ~0·9, 10 wt % clinopyroxene) leaves a mantle residue with $CaO/Al_2O_3 = 1{\cdot}2–1{\cdot}5$ and 5 wt % clinopyroxene. Further melting to exhaustion of clinopyroxene yields melts with CaO/Al_2O_3 up to 1·6 at melt fractions of 7–10%. Second-stage melting with extraction of 3–6% melt leaves some clinopyroxene (≤2 wt %) in the residue, which would reach a bulk CaO/Al_2O_3 of 2·0–3·5 (Table 9). Melting out the rest of clinopyroxene then would result in melts with CaO/Al_2O_3 above those observed in nature.

The natural limit to such a fractional melting process is the temperature necessary to produce melts with extreme CaO/Al_2O_3. Regardless of their source, the production of melts with CaO/Al_2O_3 values characteristic of ultra-calcic melts requires temperatures around 1350°C for CaO/Al_2O_3 near 1·3 and almost 1400°C for a CaO/Al_2O_3 of 1·5–1·6 [i.e. refractory peridotite in this study, wehrlite in the studies of Pickering-Witter & Johnston (2000), Kogiso & Hirschmann (2001) and Schwab & Johnston (2001)]. Addition of realistic amounts of volatiles diminishes these temperatures by only 20–30°C. The very existence of alkali-poor, hypersthene-normative ultra-calcic magmas and melt inclusions demonstrates that such temperatures are occasionally reached in all major mantle melting environments.

CONCLUSIONS

This study demonstrates that 'preconditioning' of a mantle source by melt extraction allows generation of magmas with high CaO/Al_2O_3 in equilibrium with olivine + orthopyroxene + spinel. Whatever the source CaO/Al_2O_3 in a refractory lherzolite, it will be inherited by a melt that is generated at temperatures at or above the clinopyroxene-out boundary. Residual spinel and orthopyroxene produce only a slight change to CaO/Al_2O_3 in the melt. We propose that the primitive parents of hypersthene-normative ultra-calcic magmas do not have high CaO contents, but have high CaO/Al_2O_3 and high MgO contents. Once such a parental magma is generated, olivine fractionation will increase CaO contents. SiO_2 contents of the parental melts are already high and the hypersthene-normative character will be increased by further olivine fractionation.

Most of the experiments were conducted with dissolved $CO_2 + H_2O$. If a fluid was added from a subducting slab, it would also add some minor incompatible elements to the source and could account, for example, for slightly higher K_2O and Na_2O contents than could be expected to derive from a depleted mantle source. Alternatively, CO_2 and H_2O might be added to the source through a dolomitic carbonatite melt formed in the wedge environment, which also leads to a significant increase of CaO/Al_2O_3 in the source (Green *et al*., 2004). Nevertheless, dry olivine + orthopyroxene-saturated melts are also suitable parents for ultra-calcic melts from mid-ocean ridges and ocean islands, as our dry experiments resulted in ultra-calcic melts with a CaO/Al_2O_3 to 1·48 at 1400°C. Higher temperatures and exhaustion of clinopyroxene would have caused an even higher CaO/Al_2O_3 for these melts; on the other hand, small amounts of CO_2 and H_2O as present in intraplate environments would slightly lower the temperatures required.

Our results do not constrain whether the first-stage melt extraction(s) happened immediately before the event producing the ultra-calcic melts or billions of years before. The first-stage melt extraction could occur in the same melting cycle and the ankaramites could simply be the final product of a fractional melting process. Alternatively, the first melting event could be completely unrelated to generation of the ankaramites and the diversity of magmas in a given setting would then argue for diversity of peridotitic source compositions in the mantle.

ACKNOWLEDGEMENTS

The early stage of this work greatly profited from animated discussions and e-mail exchanges with Pierre Schiano, Hugh O'Neill and Marc Hirschmann. We would also like to thank I. A. Nicholls and R. C. Price for their constructive reviews, and M. Pertermann for comments. M.S. acknowledges RSES, ANU, for a fellowship supporting his sabbatical leave at ANU during which the experiments of this study were performed. Thanks also go to all members of the experimental group at RSES for support and discussions.

REFERENCES

Baker, M. B. & Stolper, E. M. (1994). Determining the composition of high-pressure mantle melts using diamond aggregates. *Geochimica et Cosmochimica Acta* **58**, 2811–2827.

Barsdell, M. (1988). Petrology and petrogenesis of clinopyroxene-rich tholeiitic lavas, Merelava volcano, New Hebrides. *Journal of Petrology* **29**, 927–964.

Barsdell, M. & Berry, R. F. (1990). Origin and evolution of primitive island arc ankaramites from Western Epi, New Hebrides. *Journal of Petrology* **31**, 747–777.

Berry, A. J. & O'Neill, H. St. C. (2000). The oxidation state of chromium in silicate glasses as a function of oxygen fugacity, composition, temperature, and pressure. *Goldschmidt 2000. Journal of Conference Abstracts* **5**(2), 214.

Brey, G. & Green, D. H. (1977). Systematic study of liquidus phase relations in olivine melilitite + H_2O + CO_2 at high pressures and petrogenesis of an olivine melilitite magma. *Contributions to Mineralogy and Petrology* **61**, 141–162.

Cherniak, D. J. (2001). Pb diffusion in Cr diopside, augite, and enstatite, and consideration of the dependence of cation diffusion in pyroxene on oxygen fugacity. *Chemical Geology* **177**, 381–397.

Della Pasqua, F. N. & Varne, R. (1997). Primitive ankaramitic magmas in volcanic arcs: a melt-inclusion approach. *Canadian Mineralogist* **35**, 291–312.

Edgar, A. D. & Vukadinovic, D. (1992). Implications of experimental petrology to the evolution of ultrapotassic rocks. *Lithos* **28**, 205–220.

Eggins, S. M. (1993). Origin and differentiation of picritic are magmas, Ambae (Aoba), New Hebrides. *Contributions to Mineralogy and Petrology* **114**, 79–100.

Falloon, T. J., Green, D. H., Hatton, C. J. & Harris, K. L. (1988). Anhydrous partial melting of a fertile and depleted peridotite from 2 to 30 kb and application to basalt petrogenesis. *Journal of Petrology* **29**, 1257–1282.

Falloon, T. J., Green, D. H., Danyushevsky, L. V. & Faul, U. H. (1999). Peridotite melting at 1·0 and 1·5 GPa: an experimental evaluation of techniques using diamond aggregates and mineral mixes for determination of near-solidus melts. *Journal of Petrology* **40**, 1343–1375.

Green, D. H. & Falloon, T. J. (1998). Pyrolite: a Ringwood concept and its current expression. In: Jackson, I. (ed.) *The Earth's Mantle*. Cambridge: Cambridge University Press, pp. 311–378.

Green, D. H., Schmidt, M. W. & Hibberson, W. O. (2004). Island arc ankaramites: primitive melts from fluxed refractory lherzolite mantle. *Journal of Petrology* (in press).

Hirose, K. & Kawamoto, T. (1995). Hydrous partial melting of lherzolite at 1 GPa: the effect of H_2O on the genesis of basaltic magmas. *Earth and Planetary Science Letters* **133**, 463–473.

Hirose, K. & Kushiro, I. (1993). Partial melting of dry peridotites at high pressures: determination of compositions of melts segregated from peridotite using aggregates of diamond. *Earth and Planetary Science Letters* **114**, 477–489.

Hirose, K. & Kushiro, I. (1998). The effect of melt segregation on polybaric mantle melting: estimation from the incremental melting experiments. *Physics of the Earth and Planetary Interiors* **107**, 111–118.

Hirschmann, M. M., Baker, M. B. & Stolper, E. M. (1998). The effect of alkalis on the silica content of mantle-derived melts. *Geochimica et Cosmochimica Acta* **62**, 883–902.

Jaques, A. L. & Green, D. H. (1980). Anhydrous melting of peridotite at 0–15 kb pressure and the genesis of tholeiitic basalts. *Contributions to Mineralogy and Petrology* **73**, 287–310.

Kamenetsky, V. S., Crawford, A. J., Eggins, St. M. & Mühe, R. (1997). Phenocryst and melt inclusion chemistry of near-axis seamounts, Valu Fa Ridge, Lau Basin: insight into mantle wedge melting and the addition of subduction components. *Earth and Planetary Science Letters* **151**, 205–223.

Kamenetsky, V. S., Eggins, St. M., Crawford, A. J., Green, D. H., Gasparon, M. & Falloon, T. J. (1998). Calcic melt inclusions in primitive olivine at 43°N MAR: evidence for melt–rock reaction/melting involving clinopyroxene-rich lithologies during MORB generation. *Earth and Planetary Science Letters* **160**, 115–132.

Kogiso, T. & Hirschmann, M. M. (2001). Experimental study of clinopyroxenite partial melting and the origin of ultra-calcic melt inclusions. *Contributions to Mineralogy and Petrology* **142**, 347–360.

Kushiro, I. (1969). The system Forsterite–Diopside–Silica with and without water at high pressures. *American Journal of Science* **267**, 269–294.

Kushiro, I. (1996). Partial melting of a fertile mantle peridotite at high pressures: an experimental study using aggregates of diamond. In: Basu, A. & Hart, S. (eds) *Earth Processes: Reading the Isotopic Code. Geophysical Monograph, American Geophysical Union* **95**, 109–122.

Liu, X. & O'Neill, H. St. C. (2002). Accurate determination of the solidus of simplified spinel lherzolite in the system CaO–MgO–Al_2O_3–SiO_2 (CMAS) at 11 kbar: traditional and new experimental techniques. *EMPG IX. Journal of Conference Abstracts* **7**(1), 67.

Medard, E., Schmidt, M. W. & Schiano, P. (2002). High-Ca primitive liquids: partial melts of clinopyroxene-rich cumulates? *Journal of Conference Abstracts* **7**, 70.

Nickel, K. G. & Brey, G. P. (1984). Subsolidus orthopyroxene–clinopyroxene systematics in the system CaO–MgO–SiO_2 to 60 kbara re-evaluation of the regular solution model. *Contributions to Mineralogy and Petrology* **87**, 35–42.

Pickering-Witter, J. & Johnston, A. D. (2000). The effects of variable bulk composition on the melting systematics of fertile peridotitic assemblages. *Contributions to Mineralogy and Petrology* **140**, 190–211.

Schiano, P., Eiler, J. M., Hutcheon, I. D. & Stolper, E. M. (2000). Primitive CaO-rich, silica-undersaturated melts in island arcs: evidence for the involvement of clinopyroxene-rich lithologies in the petrogenesis of arc magmas. *Geochemistry, Geophysics, Geosystems* **1**, Paper number 1999G000032.

Schwab, B. E. & Johnston, A. D. (2001). Melting systematics of modally variable, compositionally intermediate peridotites and the effects of mineral fertility. *Journal of Petrology* **42**, 1789–1811.

Sigurdsson, I. A., Steinthorsson, S. & Grönvold, K. (2000). Calcium-rich melt inclusions in Cr-spinels from Borgarhraun, northern Iceland. *Earth and Planetary Science Letters* **183**, 15–26.

Slater, L., McKenzie, D., Grönvold, K. & Shimizu, N. (2001). Melt generation and movement beneath Theistareykir, NE Iceland. *Journal of Petrology* **42**, 321–354.

Sobolev, A. V. & Chaussidon, M. (1996). H_2O concentrations in primary melts from supra-subduction zones and mid-ocean ridges: implications for H_2O storage and recycling in the mantle. *Earth and Planetary Science Letters* **137**, 45–55.

Sobolev, A. V. & Danyushevsky, L. V. (1994). Petrology and geochemistry of boninites from the north termination of the Tonga Trench: constraints on the generation conditions of primary high-Ca boninite magmas. *Journal of Petrology* **35**, 1183–1211.

Suyehiro, K., Takahashi, N., Ariie, Y., Yokoi, Y., Hino, R., Shinohara, M., Kanazawa, T., Hirata, N., Tokuyama, H. & Taira, A. (1996). Continental crust, crustal underplating, and low-Q upper mantle beneath an oceanic island arc. *Science* **272**, 390–392.

Takahashi, E., Shimazaki, Y., Tsuzaki, Y. & Yoshida, H. (1993). Melting study of peridotite KLB-1 to 6·5 GPa and the origin of

basaltic magmas. *Philosophical Transactions of the Royal Society of London, Series A* **342**, 105–120.

Taylor, W. R. & Green, D. H. (1987). The petrogenetic role of methane: effect on liquidus phase relations and the solubility mechanism of reduced C–H volatiles. In: Mysen, B. O. (ed.) *Magmatic Processes and Physiochemical Principles. Geochemical Society Special Publication* **1**, 121–138.

Ulmer, P. (1989). The dependence of the Fe^{2+}–Mg cation-partitioning between olivine and basaltic liquid on pressure, temperature and composition. An experimental study to 30 kbar. *Contributions to Mineralogy and Petrology* **101**, 261–273.

Yoder, H. S. & Tilley, C. F. (1962). Origin of basaltic magmas: an experimental study of natural and synthetic rock systems. *Journal of Petrology* **3**, 342–532.